© 2021. Published by The Company of Biologists Ltd | Development (2021) 148, dev194951. doi:10.1242/dev.194951

RESEARCH ARTICLE

The histone demethylase PHF8 regulates astrocyte differentiation and function

Simona Iacobucci[1], Natalia Padilla[2,*], Martina Gabrielli[3,*], Claudia Navarro[1], Marta Lombardi[3], Marta Vicioso-Mantis[1], Claudia Verderio[3], Xavier de la Cruz[2] and Marian A. Martínez-Balbás[1,‡]

ABSTRACT

Epigenetic factors have been shown to play a crucial role in X-linked intellectual disability (XLID). Here, we investigate the contribution of the XLID-associated histone demethylase PHF8 to astrocyte differentiation and function. Using genome-wide analyses and biochemical assays in mouse astrocytic cultures, we reveal a regulatory crosstalk between PHF8 and the Notch signaling pathway that balances the expression of the master astrocytic gene *Nfia*. Moreover, PHF8 regulates key synaptic genes in astrocytes by maintaining low levels of H4K20me3. Accordingly, astrocytic-PHF8 depletion has a striking effect on neuronal synapse formation and maturation *in vitro*. These data reveal that PHF8 is crucial in astrocyte development to maintain chromatin homeostasis and limit heterochromatin formation at synaptogenic genes. Our studies provide insights into the involvement of epigenetics in intellectual disability.

KEY WORDS: PHF8, Histone demethylation, Chromatin transcription, Astrocyte differentiation, Synapse, XLID

INTRODUCTION

X-linked intellectual disability (XLID) includes a diverse group of cognitive disorders ranging from mild intellectual deficits to severe cognitive impairments (Chelly et al., 2006; Ropers and Hamel, 2005). Intellectual disability (ID), as well as other neurodevelopmental disorders, is characterized by anomalies in the establishment and function of synaptic circuits. Historically, ID research focused mainly on neurons, although astrocytes make a crucial contribution to synapse formation (Cresto et al., 2019; McGann et al., 2012), maturation and elimination (Araque et al., 2014). Only recently have genetic studies underscored the potential role of astrocytes in neurodevelopmental disorders, such as Down, Rett and Fragile X syndromes (Cresto et al., 2019). Thus, astrocyte contribution to ID is still largely unexplored.

Large-scale genetic analyses revealed that a strikingly considerable number of genes mutated in XLID encode regulators of chromatin activity and structure (Chelly et al., 2006; Kramer and van Bokhoven, 2009). In particular, gene mutation screening and linkage analysis of familial ID have identified the histone demethylase (HDM) plant homeodomain finger (PHD) protein 8 (PHF8) as a factor associated with XLID (Koivisto et al., 2007; Loenarz et al., 2010; Qiao et al., 2008). PHF8 belongs to the KDM7 family of HDMs that is formed by PHF2, PHF8 and KIAA1718 (KDM7A) in humans (Li et al., 2006). The members of this family contain an amino-terminal PHD finger that recognizes and binds methylated lysines (Fortschegger et al., 2010; Horton et al., 2010; Kleine-Kohlbrecher et al., 2010; Tsukada et al., 2010; Wen et al., 2010) and a Jumonji-C (JmjC) domain that catalyzes lysine demethylation (Fortschegger and Shiekhattar, 2011). Previous studies have demonstrated that PHF8 removes mainly mono- and dimethyl-lysine 9 on histone H3 (H3K9me1/2) and monomethyl-lysine 20 on histone H4 (H4K20me1) (Fortschegger et al., 2010; Horton et al., 2010; Kleine-Kohlbrecher et al., 2010; Liu et al., 2010). Deletions and point mutations in the PHF8 catalytic domain cause Siderius–Hamel syndrome, characterized by mild XLID with cleft lip and/or a cleft palate (Abidi et al., 2007; Koivisto et al., 2007; Laumonnier et al., 2005; Siderius et al., 1999). Moreover, PHF8 might contribute to this phenotype by targeting genes such as *JARID1C* and *MSX1* (Kleine-Kohlbrecher et al., 2010; Qi et al., 2010), which are involved in XLID and neural development, respectively; indeed, PHF8 depletion was shown to impair the neuronal differentiation of murine P19 cells (Qiu et al., 2010). In addition, *in vivo* studies demonstrated that genetic silencing of the *Phf8* homolog in zebrafish caused apoptosis of neural cells and craniofacial anomalies (Qi et al., 2010; Tsukada et al., 2010), and led to a global increase in H3K9me2 and compromised locomotion in *Caenorhabditis elegans* (Kleine-Kohlbrecher et al., 2010).

Although it is well established that PHF8 plays a role in neural differentiation, how mutations in the PHF8 catalytic domain cause ID remains unknown. Recent studies have shown that *Phf8*-null mice display deficiencies in learning and memory as a result of alterations of the RSK-mTOR-S6K pathway (Chen et al., 2018) and are resistant to anxiety- and depression-like behaviors because of dysregulation of serotonin receptor *Htr1a* and *Htr2a* expression (Walsh et al., 2017). Interestingly, the PHF8-mediated transcriptional changes are extremely subtle in neurons; this might indicate that alterations not only in neurons, but also in other cells may account for the PHF8 lack-of-function phenotype. Thus, we investigated the contribution of PHF8 to astrocyte differentiation and function at the molecular level.

Here, we show that PHF8 directs the expression of some key regulators of astrocyte differentiation, such as *Nfia*, and that depletion of PHF8 has a striking effect on synapse formation and maturation. *Phf8*-depleted astrocytes show impaired transcription of genes crucial for synaptogenesis; this phenotype can be rescued by overexpressing wild type (WT) PHF8 but not the catalytic mutant. Interestingly, PHF8 depletion or loss of catalytic activity leads to a

[1]Department of Molecular Genomics, Instituto de Biología Molecular de Barcelona (IBMB), Consejo Superior de Investigaciones Científicas (CSIC), Barcelona 08028, Spain. [2]Research Unit in Clinical and Translational Bioinformatics, Vall d'Hebron Institute of Research (VHIR), Passeig de la Vall d'Hebron, 119; E-08035 Barcelona, Spain. Institut Català per la Recerca i Estudis Avançats (ICREA), Barcelona 08018, Spain. [3]CNR Institute of Neuroscience, via Vanvitelli 32, 20129 Milan, Italy.
*These authors contributed equally to this work

‡Author for correspondence (mmbbmc@ibmb.csic.es)

M.G., 0000-0003-4958-541X; M.V., 0000-0002-4069-3951; M.A.M., 0000-0003-0173-0964

Handling Editor: James Briscoe
Received 17 July 2020; Accepted 15 April 2021

Development (2021) 148, dev194951. doi:10.1242/dev.194951

global increase in heterochromatin-associated histone marks in astrocytes. Our data suggest that the loss of PHF8 in astrocytes impairs synaptogenesis because of the formation of ectopic heterochromatin.

RESULTS

PHF8 expression during astrocyte differentiation

Analysis of publicly available data of human (Zhang et al., 2016) and mouse (Zhang et al., 2014) neural cell populations showed that astrocytes express high levels of PHF8 (Fig. 1A; Fig. S1A). Interestingly, this expression was particularly high in fetal astrocytes (Fig. 1A), suggesting a potential role of PHF8 in early events of astrocyte development. To evaluate the functional relevance of PHF8 during astrocyte differentiation, we isolated neural stem cells (NSCs) from cortices of mouse embryos at embryonic day (E) 12.5 (Estaras et al., 2012; Sun et al., 2001) and differentiated them to astrocytes following the protocol described in the Materials and Methods (Fig. 1B). After 6 days in astrocytic

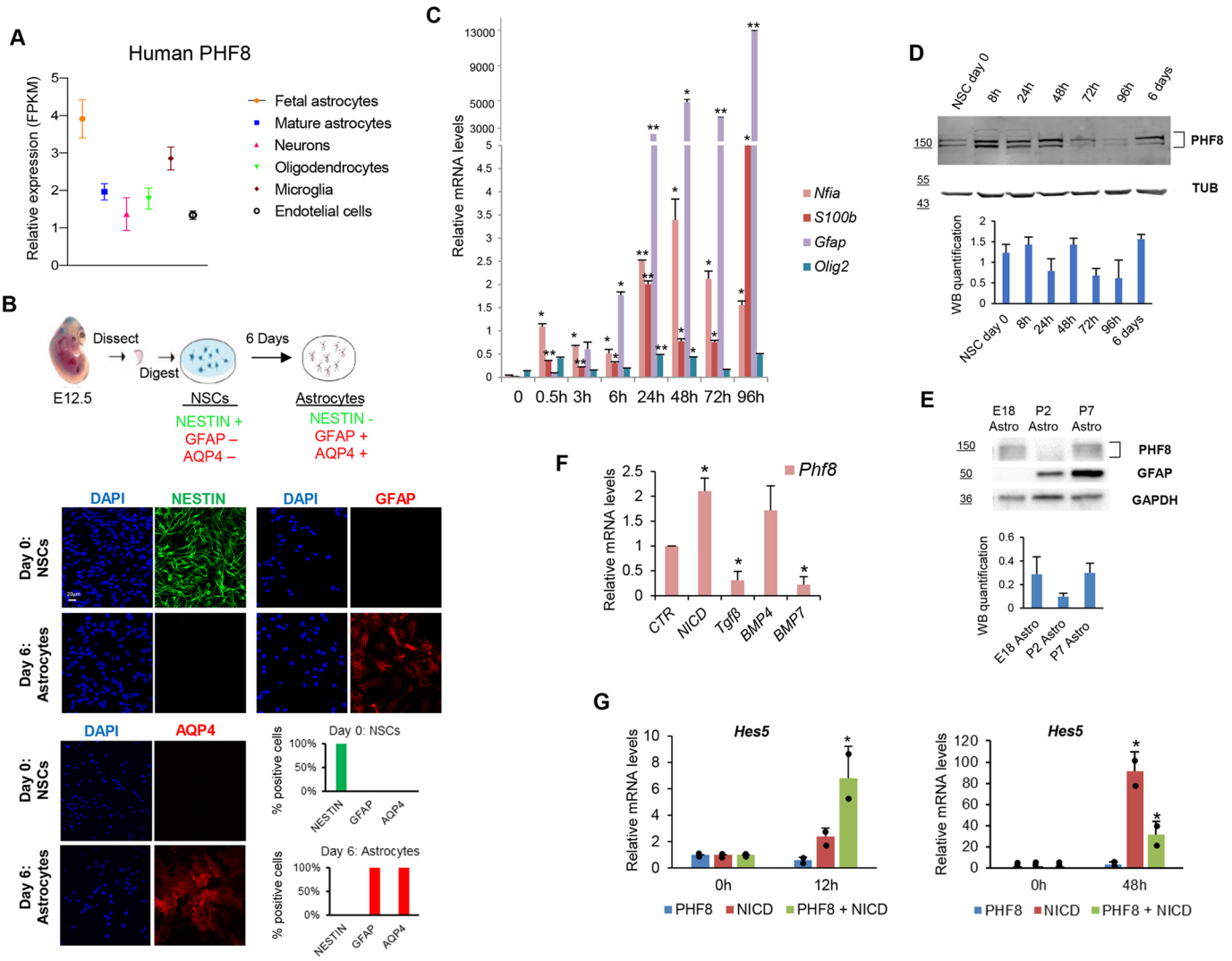

Fig. 1. PHF8 expression fluctuates during astrocyte differentiation. (A) PHF8 expression in different human neural cells. Expression level is shown by fragments per kilobase of transcript per million reads mapped (FPKM). Publicly available data from human RNA-seq experiments (http://www.brainrnaseq.org; Zhang et al., 2016). Data are mean±s.d. (B) Top: Schematic view of the model used to study the function of PHF8 during astrocyte differentiation. Bottom: Immunostaining assay of NSCs (day 0) and astrocytes (day 6) using nestin, AQP4 and GFAP antibodies and DAPI. Data shown are representative of three biological independent experiments; more than 50 cells were quantified per replicate. The graphs represent the percentage of cells expressing GFAP, AQP4 or nestin at day 0 (NSCs, green) and day 6 (astrocytes, red). (C) NSCs were maintained in astrocytic differentiation medium for different lengths of time. Total RNA was prepared at the indicated times and the levels of *Nfia*, *S100b*, *Gfap* and *Olig2* were determined by qPCR. Expression values were normalized to the housekeeping gene *Gapdh*; values shown are relative to time 0 h. *Olig2* mRNA was used as a negative control. Data are mean±s.d.; n=3 biological replicates. *P<0.05; **P<0.01. (D) NSCs were maintained in astrocytic differentiation medium for the indicated times. Total protein extracts were prepared and the PHF8 levels were determined by immunoblot. Alpha-tubulin antibody (TUB) was used as the loading control. Data are mean±s.d.; blot is representative of two biological independent experiments. (E) PHF8 western blot assays of MACS-isolated astrocytes from E18, P2 and P7 mouse brain. GAPDH antibody was used as a loading control. Data are mean±s.d.; blot is representative of two biological independent experiments. (F) HEK 293T cells were transfected with NICD, Smad3S/D (the constitutive active form of Smad3), BMP7, BMP4 or empty vector (CTR) as indicated. Total mRNA was purified and the *PHF8* levels were determined by qPCR. Expression values were normalized to the housekeeping gene *GAPDH*. Data are mean±s.d.; n=3 independent biological replicates. *P<0.05. (G) HEK 293T cells were transfected with a vector expressing *Phf8* together or not with NICD. Total mRNA was purified and the *HES5* levels at 12 h (left) and 48 h (right) were established by qPCR. Values shown are relative to time 0 h. Expression values were normalized to the housekeeping gene *GAPDH*. Data are mean±s.d.; n=2 independent biological replicates. Values from each are indicated by dots. *P<0.05. Scale bar: 20 µm.

Development (2021) 148, dev194951. doi:10.1242/dev.194951

medium, almost 100% of NSCs had lost expression of the progenitor marker nestin and acquired high levels of the astrocyte-associated markers glial fibrillary acidic protein (GFAP) and aquaporin-4 (AQP4) (Fig. 1B). No signal for β-Tubulin 3 (TUBβ3), a marker of neuronal differentiation, was noticed at that time (Fig. S1B), although some TUBβ3-expressing cells were detected during early differentiation timepoints (Fig. S1B). Accordingly, a progressive increase in *Nfia* and *S100b* expression was detected throughout the neuronal differentiation process (Fig. 1C). Immunostaining of H4K20me1/3, H3K27me3 and H3K9me2 histone marks associated with heterochromatin formation also increased during this differentiation (Fig. S1C).

To gain insight into the role of PHF8 in astrocyte differentiation, we analyzed *Phf8* expression during this process. The results showed an increase in PHF8 protein levels during early differentiation and in differentiated astrocytes (6 days of differentiation) (Fig. 1D). PHF8 upregulation *in vivo* was demonstrated by western blot assays of magnetic-activated cell sorting (MACS)-isolated astrocytes from early development (E18) and intact postnatal (P) mouse brain (P2 and P7) (Fig. 1E). These data suggest a potential contribution of PHF8 to both astrocyte differentiation and function.

Next, we sought to identify the signaling pathway that could be responsible for *Phf8* upregulation during astrocyte differentiation. Given that Notch, TGFβ and BMP signals are involved in astrocyte development, we activated these pathways and determined the *Phf8* mRNA levels by qPCR. The results showed a clear *Phf8* induction after transfection of the Notch intracellular domain (NICD) (Fig. 1F). The Notch pathway is crucial for astrocyte differentiation induction (Ge et al., 2002; Martini et al., 2013); thus, we investigated whether PHF8 modulates Notch activity. To do so, we overexpressed *Phf8* upon Notch activation (by NICD expression) and analyzed the expression of the well-known Notch target *Hes5* by qPCR. PHF8 facilitated Notch target activation over short time frames, but inhibited it over longer time frames (Fig. 1G). This repression was also observed in overexpression and depletion experiments using a luciferase reporter vector fused to the *Hes5* promoter (Fig. S1D,E).

Altogether, these data demonstrate that PHF8 expression is modulated during astrocyte differentiation. Moreover, they suggest the existence of a regulatory feedback loop between PHF8 and Notch signaling.

PHF8 regulates transcription during astrocyte differentiation

To gain further understanding of the function of PHF8 in astrocytes, we analyzed the PHF8-dependent transcriptional profile by RNA-sequencing (RNA-seq). To this end, NSCs were transduced with a lentivirus containing either a specific PHF8 short hairpin (sh)RNA that efficiently decreased the PHF8 protein levels (Fig. S2A) or a control shRNA (see Materials and Methods). Next, control (CTR) and PHF8-depleted (PHF8-KD) NSCs were differentiated into astrocytes (6 days of differentiation) (Fig. 2A). Astrocytes derived from PHF8-KD NSCs (Astro PHF8-KD) exhibited decreased PHF8 transcription compared with those from control NSCs (Astro-CTR), as indicated by qPCR (Fig. 2A, bottom panel). The transcriptional profiles of two Astro-CTR and two Astro PHF8-KD samples (Fig. S2B,C) showed that 4987 transcripts had significantly altered expression [$\log_2$ fold change (FC) >0.5 and <−0.5, respectively; P<0.08] in two biologically independent experiments (Fig. 2B,C). Among these transcripts, 2899 (58%) were downregulated and 2087 (42%) were upregulated upon PHF8 depletion. When the $\log_2$ FC was increased to 2, the percentage of downregulated genes (694) increased to 76% (Fig. 2D; Fig. S2D), in agreement with the activator role proposed for PHF8. Changes in the expression of some selected genes were validated by qPCR (Fig. S2E).

To further characterize the difference between CTR and PHF8-KD astrocytes, we performed a gene ontology (GO) enrichment analysis of regulated genes to identify those biological processes most sensitive to PHF8 depletion. The analysis revealed changes in genes related to biological processes involved in synapse formation and maturation (Fig. 2E), including the astrocytic genes *Gpc4*, *Sparc*, *Thbs1*, *Nrxn1*, *Pcdh8* and *Sdc4* (Cheng et al., 2016; Farhy-Tselnicker et al., 2017; Kucukdereli et al., 2011; Singh et al., 2016) (Fig. 2F). Interestingly, synaptic genes were both downregulated and upregulated in PHF8-depleted astrocytes (Fig. S2F), although downregulated genes showed higher FC values. Importantly, 57% of the astrocytic genes involved in neuron-astrocyte interplay at synapses (Hillen et al., 2018) were affected in PHF8-KD astrocytes (Fig. S2F,G), suggesting that the synapse might be altered. In addition, some Notch targets (*Notch3*, *Hes5*, *Dll3*, *Dll1* and *Cd44*) were misregulated in PHF8-KD astrocytes (Fig. S2H,I). Interestingly, the Notch signaling pathway is crucial for the induction of astrocyte differentiation (Ge et al., 2002; Martini et al., 2013). Finally, an essential gene for astrogenesis, *Nfia* (Deneen et al., 2006), was downregulated in PHF8-depleted astrocytes (Fig. S2E,J), pointing to a significant role of PHF8 in astrocytic differentiation.

Altogether, these data demonstrate that PHF8 facilitates the transcription of astrogenic and synaptogenic genes.

PHF8 binds to astrogenic and synaptogenic genes

To gain insight into the contribution of PHF8 to gene regulation, we next determined its biological substrates by performing chromatin immunoprecipitation coupled with sequencing (ChIP-seq) in astrocytes after 6 days of differentiation (Fig. 3A). Upon normalization to the input, 8401 peaks (P=0.001) were detected in ChIP data for PHF8 (Fig. 3B). The analysis of the genomic distribution of PHF8 peaks revealed that 46.8% of the peaks localized on distal intergenic regions (see example in Fig. S3A). The remaining 53% were located along the genome and were particularly enriched at introns (Fig. 3B,C). Interestingly, the PHF8 distribution in postmitotic astrocyte cells was noticeably different to that previously described in embryonic stem cells (ESCs), in which the majority of the PHF8-binding sites resided at promoters (Fig. S3B). Comparing PHF8 genomic location in astrocytes and ESCs, we observed that the peaks at promoters in ESCs corresponded to those at introns and intergenic regions in astrocytes (Fig. S3B). GO analysis of PHF8-bound regions indicated that PHF8 was associated with genes involved in neural development, particularly in astrogenesis (*Nfia*) and synaptogenesis (*Sparc* and *Gpc4*), among others (Fig. 3D).

To better understand how PHF8 is targeted to chromatin, we performed bioinformatics analysis and identified that one of the most statistically significant predicted PHF8-binding sites was the RBPJ1 DNA-binding motif (Fig. 3E). RBPJ1 is an effector of the Notch signaling pathway, which is essential in astrocyte differentiation (Ge et al., 2002; Martini et al., 2013). Interestingly, RBPJ1 motif and PHF8 binding were identified at the *Phf8* gene (Fig. 3F), supporting the idea that PHF8, in addition to regulating Notch targets (Fig. S2G,H), is itself a target. In fact, the RBPJ1-PHF8 interaction has been previously identified in another cellular context (Yatim et al., 2012). To reinforce these data, we performed GO analysis of the PHF8 and RBPJ1-bound regions; the results showed that they bind to genes involved in synapse assembly and

Development (2021) 148, dev194951. doi:10.1242/dev.194951

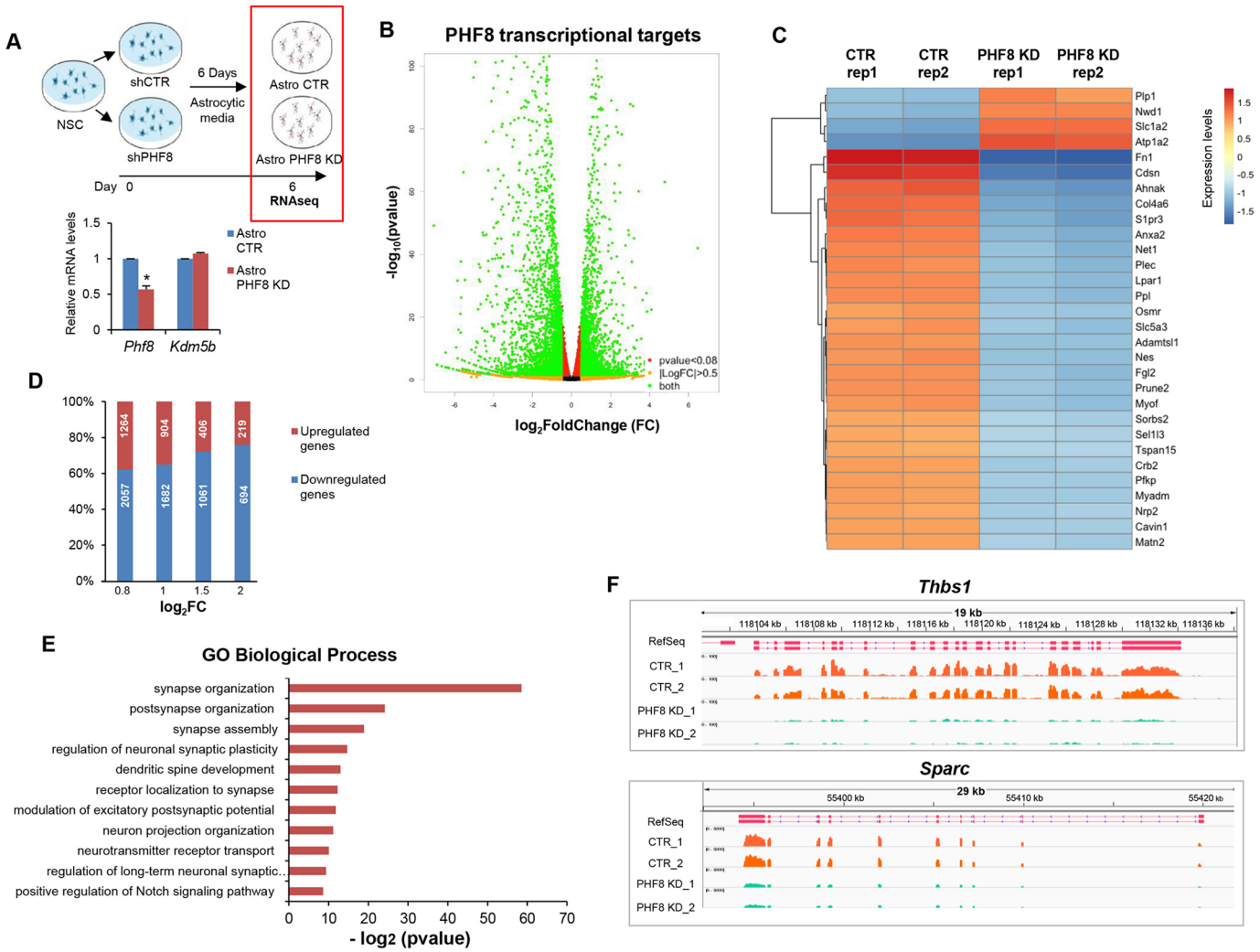

Fig. 2. PHF8 regulates transcription in astrocytes. (A) Schematic of the experiment to study the transcriptional profile of PHF8 in astrocytes (top panel). NSCs were infected with lentivirus expressing either control shRNA (shcontrol) or shRNA specific for PHF8 (shPHF8). After 6 days in astrocytic medium, total RNA was purified and the *Phf8* levels were determined by qPCR. Expression values were normalized to the housekeeping gene *Gapdh*. Data are mean±s.d.; n=3 independent biological replicates. *P<0.05. (B) Volcano plot representing PHF8 transcriptional targets identified by RNA-seq in Astro-CTR and Astro PHF8-KD. The green dots represent all genes with P<0.08 and a $\log_2$ FC >0.5 and <−0.5. (C) Heat map showing the top-30 regulated genes identified by RNA-seq in shcontrol and shPHF8 NSCs. Two biological replicates of shPHF8 cells were used for RNA-seq. All genes showed P<0.08 and a $\log_2$ FC >0.5 and <−0.5. (D) Percentage and number of upregulated and downregulated genes in Astro PHF8-KD compared with Astro-CTR with P<0.08 and classified by increasing $\log_2$ FC. (E) GO analysis showing the biological processes associated with the PHF8-regulated genes (P<0.08 and $\log_2$ FC >0.5 and <−0.5) was performed using as a background the whole *Mus musculus* genome. (F) Integrated Genomics Viewer (IGV) capture showing RNA levels in Astro-CTR and Astro PHF8-KD in *Thbs1* and *Sparc*.

function (Fig. S3C). PHF8 ChIP-seq was validated by qPCR analysis of seven randomly chosen genes (Fig. S3D). Moreover, by ChIP qPCR, we confirmed the binding of PHF8 to genes essential for astrocyte differentiation and function (*Nfia* and *Sparc*) during early stages of differentiation (day 1) (Fig. S3E).

Next, we identified the direct transcriptional targets of PHF8 by comparing the genes bound by PHF8 in the ChIP-seq experiment (4254) with the transcriptional profile ($\log_2$ FC >0.5 and <−0.5, respectively; P<0.08, 4986 transcripts). Among the genes bound by PHF8, 867 (20.3%) showed a PHF8 dependency for transcriptional regulation in the RNA-seq experiment (Fig. 3G). GO analysis of the PHF8-direct target genes showed that the most enriched terms were again related to astrocytic differentiation and synapse assembly and function (Fig. 3H).

Collectively, these data show that PHF8 regulates genes related to astrogenesis and synaptogenesis in astrocytes.

PHF8 depletion alters the astrocyte transcriptional profile

Given that PHF8 regulates the expression of key genes involved in astrocyte differentiation, we explored whether PHF8 depletion alters astrocyte differentiation. Immunostaining for the well-known astrocytic markers GLAST, GFAP, GLT-1 and AQP4 revealed that PHF8 depletion caused a decrease in GFAP protein expression, with no alteration in the other astrocytic markers (Fig. 4A). We also tested for immunoreactivity of other neural cell markers: oligodendrocytes (OLIG2, NG2 and GPR17), neurons (TUBβ3), microglia (IBA1) and NSCs (nestin) (Fig. S4A). A percentage of Astro PHF8-KD was positive for either TUBβ3 (13%) or OLIG2 (33%) (Fig. S4A). Notably, under our differentiation conditions, 12% of Astro-CTR expressed OLIG2, whereas this was higher in Astro PHF8-KD (33%). The lack of signal for other oligodendrocyte markers (GPR17 and NG2) (Fig. S4A) and the presence of astrocytic markers (GLAST, GLT-1 and AQP4) (Fig. 4A) indicated

Development (2021) 148, dev194951. doi:10.1242/dev.194951

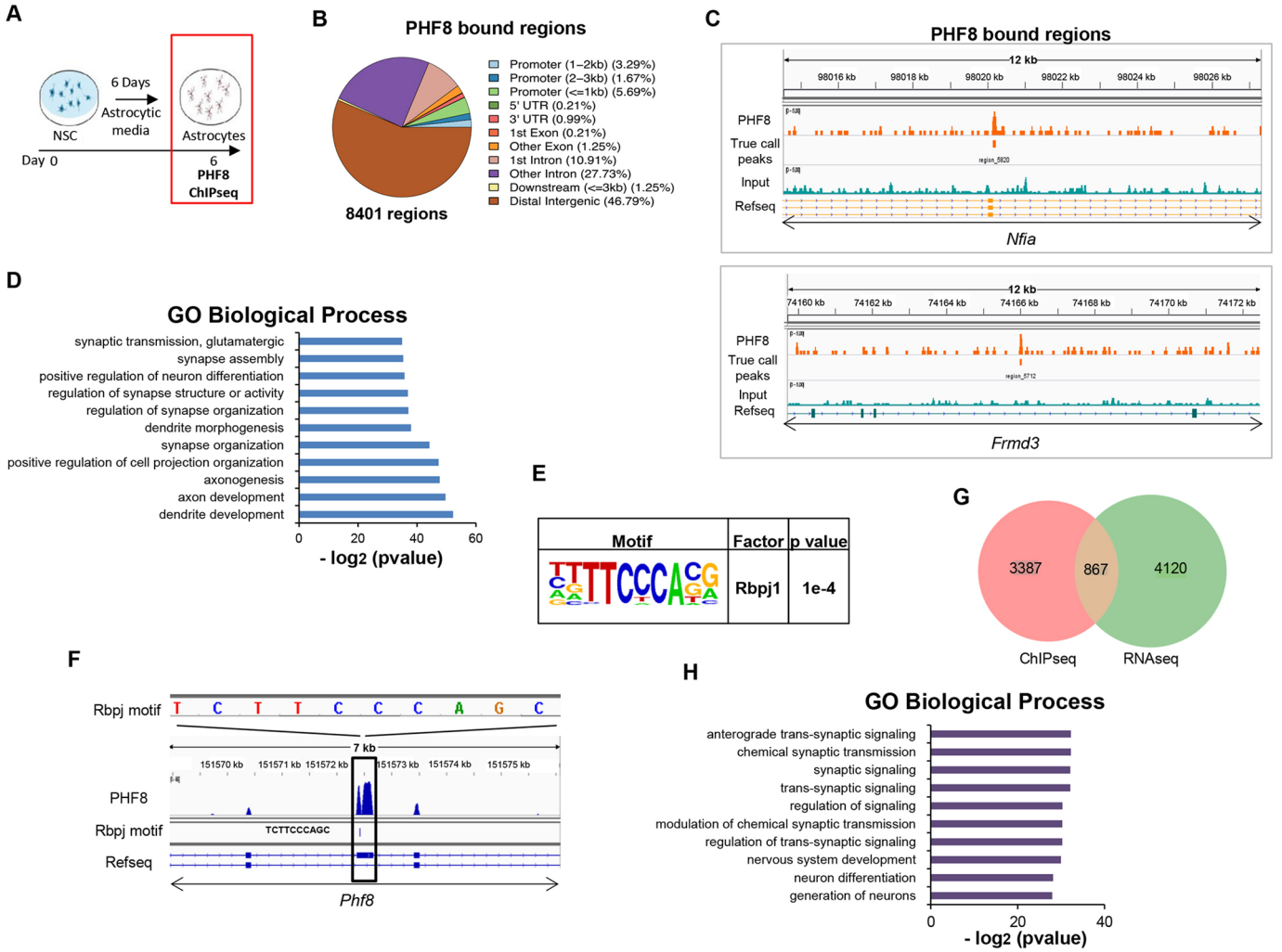

Fig. 3. PHF8 binds to astrogenic and synaptogenic genes. (A) Schematic of the ChIP-seq experiment to identify the binding sites of PHF8 in astrocytes. PHF8 antibody used for immunoprecipitation was previously used in ChIP assays (see Materials and Methods). (B) Genomic distribution of PHF8 ChIP-seq peaks in astrocytes. In total, 8401 regions were identified. (C) Integrated Genomics Viewer (IGV) captures showing PHF8 peaks in *Nfia* and *Frmd3* in astrocytes. (D) GO analysis showing the biological processes associated with the PHF8-bound genes (4254) using as a background the whole *Mus musculus* genome. (E) Motif enrichment analysis of PHF8 ChIP-seq peaks in astrocytes using 'Homer known motif' showing an enriched motif. (F) IGV captures showing PHF8 peaks and the RBPJ1-binding motif in *Phf8* in astrocytes. (G) Venn diagram showing overlap between PHF8-bound genes (4254) and PHF8 transcriptional targets with P<0.08 and $\log_2$ FC>0.5 and <−0.5 (4987 transcripts). Of the PHF8-bound genes identified by ChIP-seq, 20.3% were differentially expressed by RNA-seq. (H) GO analysis showing the biological processes associated with the PHF8-direct target genes using as a background the whole *Mus musculus* genome.

that these cells were not oligodendrocytes. Interestingly, the TUBβ3 marker was not detected in PHF8-KD astrocytes after a longer differentiation time (25 days), suggesting a delay in the differentiation process (Fig. S6C). Moreover, a small percentage of Astro PHF8-KD expressed multiple lineage markers [TUBβ3 and GLAST (9.6%); OLIG2 and GLAST (33.0%)] (Fig. S4B). To further understand the nature of astrocytes developed from PHF8-depleted NSCs, we compared the transcriptional profile of NSCs (GSE88173; ENCODE Project Consortium, 2012) with those of Astro-CTR and Astro PHF8-KD. Cells resulting from differentiation upon PHF8 depletion had an astrocyte signature, although they misexpressed some genes compared with control astrocytes (Fig. 4B). Moreover, the transcriptional profiles of both Astro-CTR and Astro PHF8-KD were clearly different from those of oligodendrocytes (Fig. S4C) or neurons (Fig. S4D). Altogether, these data suggest that PHF8-depleted NSCs differentiated *in vitro* into astrocytes that showed a distinct transcriptional profile compared with that of control astrocytes.

A possibility that could explain the differences observed in transcription is that the levels of PHF8 contribute to astrocyte heterogeneity. To explore this hypothesis, we analyzed PHF8 expression in the five astrocyte subtypes defined by Batiuk and collaborators (Batiuk et al., 2020). Given that these data were obtained from cortex and hippocampus, they are the most appropriate *in vivo* model to compare with our cortical NSC-derived astrocytes. The results indicated that PHF8 was expressed at similar levels in astrocyte subtypes (Fig. S5A). In addition, we sought to determine whether PHF8 depletion primes any enrichment of the subtypes defined by Batiuk and collaborators. Considering that the identified astrocyte subtypes are characterized by the unique expression of transcripts, we analyzed whether the genes upregulated in PHF8-depleted astrocytes were significantly enriched in any of the five astrocyte groups. No significant enrichment on any population was observed (Fig. S5B), suggesting that, upon PHF8 depletion, a reshaped transcriptional profile was obtained that did not correspond to any defined astrocyte subtypes *in vivo*. Altogether, these data

Development (2021) 148, dev194951. doi:10.1242/dev.194951

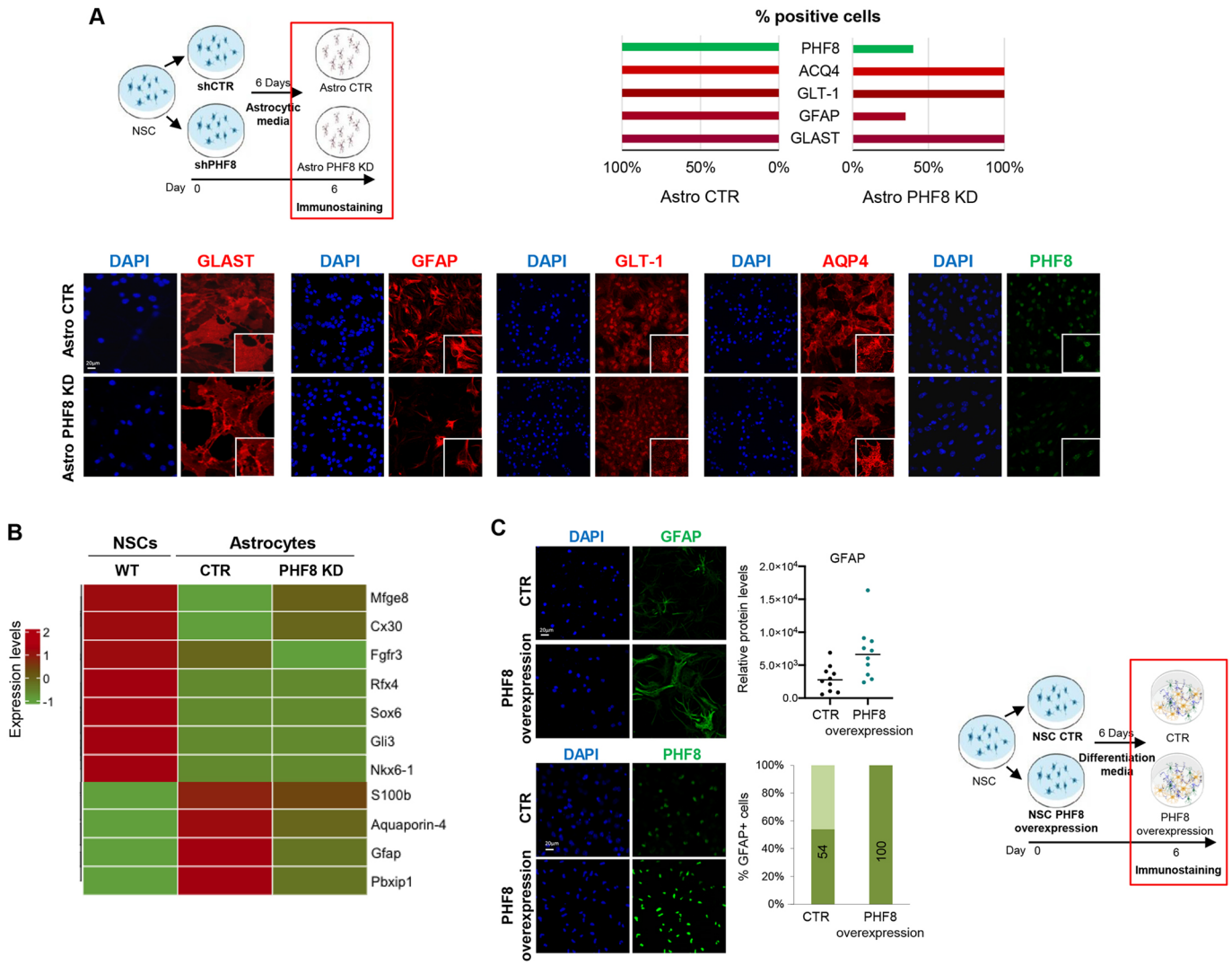

Fig. 4. PHF8-depleted NSCs differentiate into distinct astrocytes. (A) Control and PHF8-depleted NSCs were differentiated to astrocytes over 6 days to generate Astro-CTR and Astro PHF8-KD, respectively. Cells were fixed and stained with GLAST, GFAP, GLT-1, AQP4 and PHF8 antibodies and DAPI. The percentage of cells expressing these markers in each population is shown. (B) Heat map showing astrocytic gene expression identified by RNA-seq in Astro-CTR and Astro PHF8-KD compared with NSCs (GSE88173). All the genes showed $P<0.08$ and $\log_2$ FC >0.5 and <−0.5. (C) Control and PHF8-overexpressing NSCs were maintained in medium without growing factors for 6 days (see schematic). Cells were fixed and stained with GFAP antibody and DAPI. The relative levels of GFAP (determined by ImageJ) per cell and percentage of GFAP-expressing cells are shown. Images are representative of at least three biological independent experiments. Scale bars: 20 µm.

suggest that PHF8 did not contribute to generate astrocyte heterogeneity *in vitro*; however, more definitive studies are required to understand this complex issue fully.

We next investigated the capacity of Astro PHF8-KD to resume proliferation and maintain the stem cell state upon differentiation. We first compared the transcriptional profile of NSCs (GSE88173; ENCODE Project Consortium, 2012) with that of Astro-CTR or Astro PHF8-KD; Astro PHF8-KD did not express either proliferation- or stemness-related genes (Fig. S5C). Moreover, immunostaining assays did not reveal a signal for the progenitor marker nestin in Astro PHF8-KD (Fig. S4A). Finally, the ability of Astro PHF8-KD to proliferate was analyzed; the data revealed that these cells lost the ability to enter the cell cycle (as Astro CTR) under the differentiation conditions used in the study (Fig. S5D). Altogether, these data suggest that PHF8-depleted NSCs differentiate into distinct astrocytes.

Next, we investigated the contribution of *Phf8* to astrocytic fate, by establishing a NSC line that overexpressed PHF8 in an inducible manner and culturing the cells in a medium without growth factor. Under basal *Phf8* expression and without growth factor, NSCs differentiated into neurons, astrocytes and oligodendrocytes, as expected (Jori et al., 2007). However, when *Phf8* overexpression was induced, a clear increase in GFAP-, but not OLIG2-expressing cells was observed (Fig. 4C; Fig. S5E), indicating that PHF8 promotes NSC differentiation towards astrocytes.

PHF8 depletion impairs neuronal synapse

Given that PHF8 depletion led to profound defects in synaptogenic gene expression, we next investigated the function of astrocytic PHF8 in synapse formation. We cultured primary hippocampal neurons on PHF8-depleted or control astrocytes and quantified the density and function of excitatory synapses. Control or PHF8-depleted NSCs were first differentiated towards astrocytes for 10 days. Then, primary neurons were plated on the differentiated cells and maintained in co-culture for 14 days, to analyze the density of excitatory synapses and measure basal synaptic transmission (Fig. 5A). Immunofluorescence

Development (2021) 148, dev194951. doi:10.1242/dev.194951

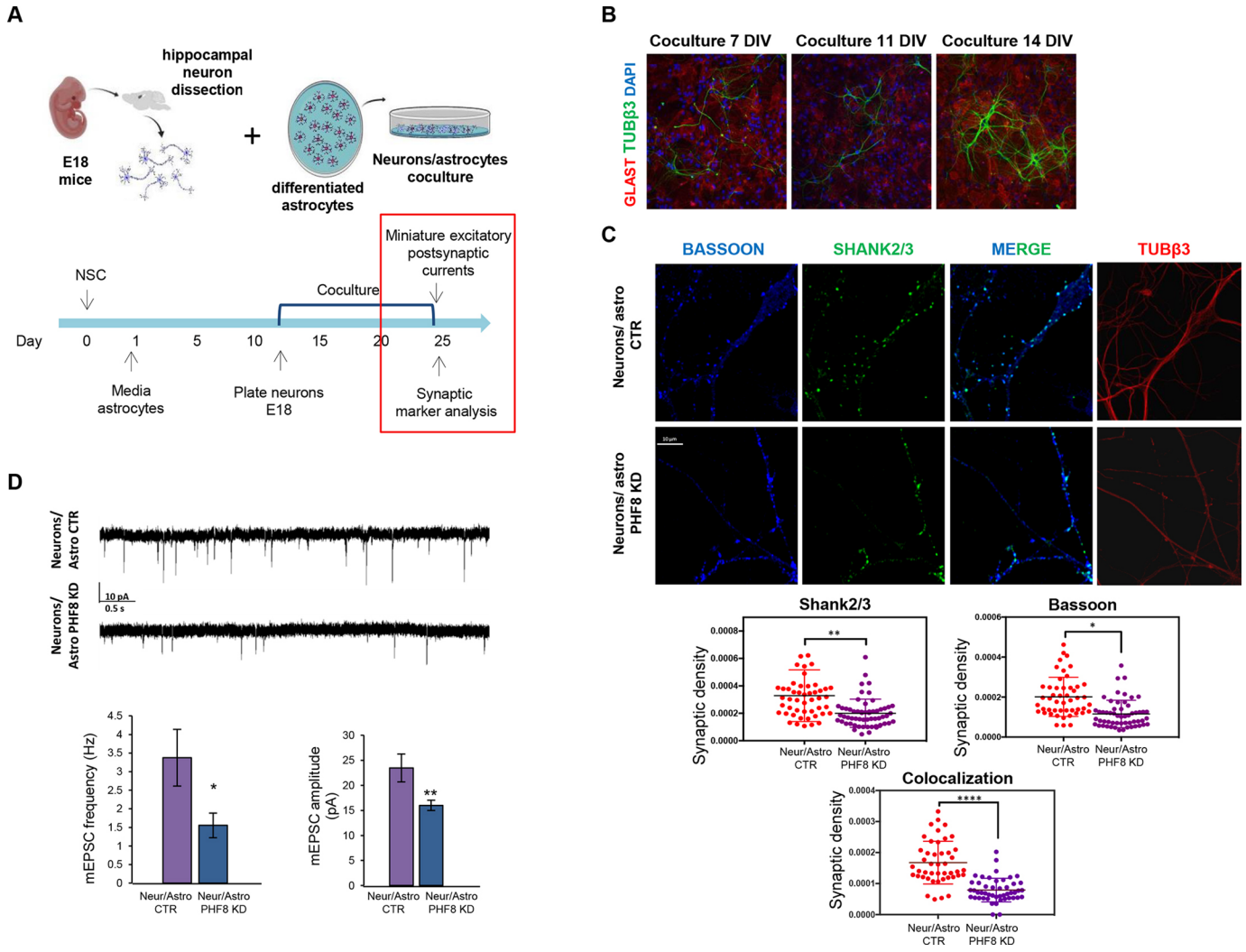

Fig. 5. PHF8 depletion impairs neuronal synapse formation. (A) Schematic of the neuron/astrocyte co-culture experiment. (B) Immunostaining assay showing GLAST, TUBβ3 and DAPI levels in co-cultures after 7, 11 and 14 DIV. (C) Immunostaining showing bassoon and SHANK2/3 staining in neurons cultured on Astro-CTR or Astro PHF8-KD (top). The synaptic density was determined by the colocalization of both markers (bottom). Data shown are representative of three biological independent experiments; more than 50 cells were quantified per replicate. **P*<0.05, ***P*<0.01, *****P*<0.0001. (D) Representative traces of mEPSCs from neurons cultured on astrocytes CTR or PHF8 KD and histogram showing the mean frequency (*P*=0.042 Mann–Whitney Rank Sum Test) and amplitudes of mEPSCs (*P*=0.009 Mann–Whitney Rank Sum Test). Data are mean±s.d.; **P*<0.05, ***P*<0.01. Scale bars: 20 µm in B; 10 µm in C.

analysis of the co-cultures for TUBβ3 revealed progressive enlargement of the neuron cell bodies and maturation of the dendritic tree over time, at 7, 11 and 14 days *in vitro* (DIV) (Fig. 5B). No differences in neuron maturation or survival were detected between neurons co-cultured with PHF8-KD versus Astro-CTR (Fig. S6A,B). Finally, the maintenance of astrocyte identity after 25 days in culture was confirmed by immunostaining assays using AQP4, GLAST, TUBβ3 and OLIG2 markers (Fig. S6C).

To prove the involvement of astrocytic PHF8 in synapse formation, we first analyzed the density of excitatory synapses. Immunostaining for the presynaptic active zone marker bassoon and the postsynaptic density marker SHANK2 showed a significant decrease in the density of both pre- and postsynaptic puncta as well as of juxtaposed pre- and postsynaptic terminals (normalized per dendritic length, see Materials and Methods), in neurons co-cultured with PHF8-KD astrocytes compared with neurons co-cultured with Astro-CTR (Fig. 5C). As a further control, we examined synaptic density in neurons cultured in the absence of astrocytes. The analysis showed a similar decrease in the density of bassoon-positive presynaptic terminals in purified neurons and neurons co-cultured with PHF8-depleted astrocytes compared with neurons co-cultured with Astro-CTR (Fig. S6D). The same held true for SHANK2-positive postsynaptic terminals and bassoon/SHANK2 colocalizing puncta (Fig. S6D).

To evaluate the impact of astrocytic PHF8 depletion on synaptic transmission, we measured miniature excitatory postsynaptic currents (mEPSCs), through whole-cell patch-clamp electrophysiological recordings, on 14-day-old neurons co-cultured with either control or PHF8-depleted astrocytes. Importantly, only neurons with similar resting membrane potentials were analyzed. mEPSC analysis revealed a significant decrease in both the frequency and amplitude of the miniature excitatory events upon astrocytic PHF8 depletion (Fig. 5D). A variation in mEPSC frequency is usually related to presynaptic changes leading to altered probability of neurotransmitter release, or to a change in the number of synapses, in line with immunofluorescence analysis for pre- and postsynaptic markers

Development (2021) 148, dev194951. doi:10.1242/dev.194951

reported herein. By contrast, variation in mEPSC amplitude is probably the result of postsynaptic modifications, such as an altered number of postsynaptic receptors.

Altogether, these data demonstrate that PHF8 deficiency in astrocytes induces profound alterations in the formation and function of excitatory synapses *in vitro*.

PHF8 maintains low levels of H4K20me1/3 at astrogenic and synaptogenic genes

Previous studies have shown that H4K20me1 is the main substrate of PHF8 demethylating activity (Liu et al., 2010). Thus, using immunofluorescence analysis, we evaluated the impact of PHF8 depletion on H4K20me1 global levels in astrocytes, finding a slight increase in H4K20me1 levels (Fig. 6A; Fig. S7A), as previously demonstrated in other cellular contexts (Liu et al., 2010). Given that the H4K20me1 mark serves as substrate for the histone methyltransferase SUV420H1 (KMT5B), we also tested the levels of H4K20me3 and found a clear increase in the H4K20me3 heterochromatic mark. Intriguingly, both the intensity and number of H4K20me3 foci increased upon PHF8 depletion (Fig. 6B), whereas no changes in other histone marks associated with transcriptional activation, such as H3K4me3, were detected (Fig. S7B).

Given that depletion of PHF8 in astrocytes led to an increase in global H4K20me3–heterochromatin-related marks, we investigated whether PHF8 is important in preventing the accumulation of H4K20me at PHF8-regulated genes during astrocyte differentiation. We chose two PHF8-target genes identified by ChIP-seq and essential for astrogenesis (*Nfia*) and synaptogenesis (*Sparc*) and tested the effect of PHF8 depletion on H4K20me1 levels in NSCs,

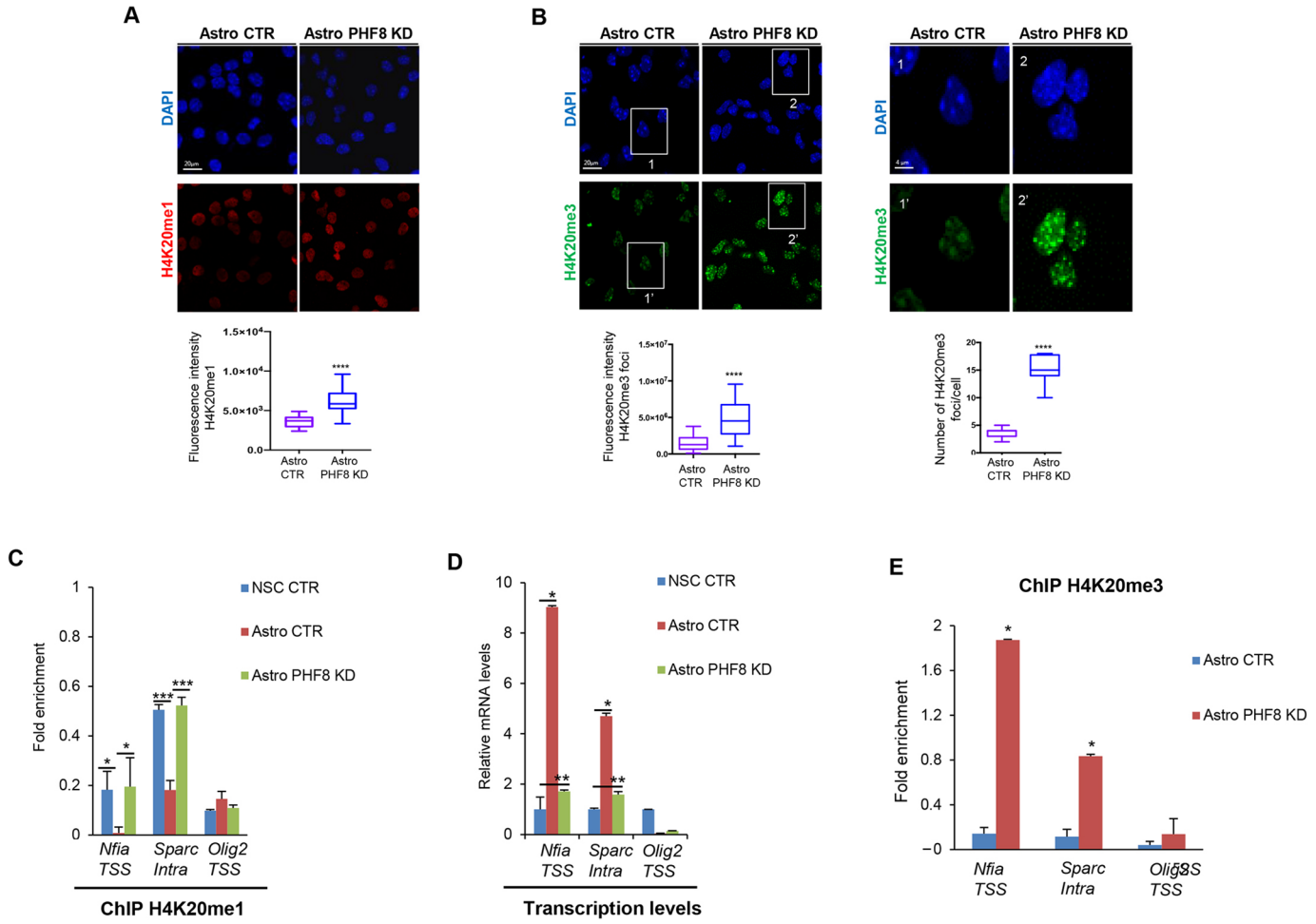

Fig. 6. PHF8 maintains low levels of H4K20me1/3 at key astrogenic and synaptogenic genes. (A,B) Astro-CTR and Astro PHF8-KD were fixed and immunostained using H4K20me1 (A) and H4K20me3 (B) antibodies and DAPI. Magnifications show H4K20me3 foci in Astro-CTR and Astro PHF8-KD. Cell fluorescence for H4K20me1 and H4K20me3 staining and H4K20me3 foci was measured using ImageJ. Images are representative of at least three biological independent experiments. More than 30 cells per population were quantified. Box plots represent the quantification of the fluorescence intensities and the number of H4K20me3 foci/cell in Astro-CTR and Astro PHF8-KD. Boxes show magnified regions on the right. ****P<0.0001. (C) Levels of H4K20me1 histone marks in NSCs, Astro-CTR and Astro PHF8-KD were determined by ChIP-qPCR at the indicated genes. The *Olig2* TSS region devoid of H4K20me1 was used as a negative control. Data from qPCR were normalized to the input, the IgG values were subtracted and the final data were expressed as fold enrichment over the values obtained in the shCTR. 'Intra' refers to the intragenic region identified in the PHF8 ChIP-seq assays. Data are mean±s.d.; *P<0.05; ***P<0.001. (D) Expression levels of the indicated genes in NSCs, Astro-CTR and Astro PHF8-KD were determined by qPCR. Values were normalized to the housekeeping gene *Gapdh* and are shown relative to time 0 h. *Olig2* mRNA was used as a negative control. Data are mean±s.d.; n=3 independent biological replicates. *P<0.05; **P<0.01. (E) The levels of H4K20me3 in Astro-CTR and Astro PHF8-KD were determined by ChIP-qPCR. The *Olig2* TSS region was used as a negative control. Data from qPCR were normalized to the input, the IgG values were subtracted and the final data were expressed as fold enrichment over the values obtained in shCTR. 'Intra' refers to intragenic region identified in the PHF8 ChIP-seq assay. Errors bars represent s.d. *P<0.05. Scale bars: 4 µm in B (magnifications); 20 µm in B (main images). TSS, transcription start site.

Development (2021) 148, dev194951. doi:10.1242/dev.194951

control astrocytes and PHF8-depleted astrocytes by ChIP-qPCR. A clear decrease in H4K20me1 mark was noticed upon astrocyte differentiation (Fig. 6C) (comparing NSCs and Astro-CTR) that correlated with gene activation (Fig. 6D); no changes at the *Olig2* promoter (a non-PHF8 target used as a negative control) were observed (Fig. 6C). Interestingly, there was no decrease in H4K20me1 in PHF8-depleted astrocytes (Fig. 6C), indicating that PHF8 catalytic activity might be involved in their regulation. We also analyzed the consequences of PHF8 depletion on H4K20me3 levels. A clear increase in H4K20me3 was observed in PHF8 KD cells (Fig. 6E), in agreement with the increased global levels (Fig. 6B). Given that PHF8 also targets the H3K9me2 histone mark (Horton et al., 2010; Kleine-Kohlbrecher et al., 2010), we analyzed whether PHF8 acts by demethylating H3K9me2 on the regions identified by ChIP-seq. PHF8 was not found to be responsible for maintaining low levels of H3K9me2 at the analyzed genes in astrocytes, because no increase in H3K9me2 was observed upon PHF8 depletion (Fig. S7C).

PHF8 HDM activity is important for astrocyte differentiation

Given that changes in H4K20me1/3 levels correlated with transcriptional changes in genes involved in astrocytic differentiation and synapses (Fig. 6C-E), we assessed the role of PHF8 HDM activity in the observed phenotypes. We established PHF8-KD NSC cell lines that overexpressed either WT PHF8 or a PHF8 mutant lacking HDM activity (mutant H247A) (see Materials and Methods) (Fig. S7D). First, we rescued the defects on astrocyte differentiation by analyzing GFAP protein in differentiated cells. GFAP expression was recovered upon PHF8 WT overexpression, but not upon overexpression of the catalytic mutant (Fig. 7A). Next, we tested the role of the catalytic activity in the control of synaptic and astrocytic gene expression. qPCR demonstrated that PHF8 WT, but not the PHF8 mutant, was able to rescue the expression levels of the tested astrogenic and synaptogenic genes regulated by PHF8 during differentiation without affecting the expression of *Kdm5b* (used as a negative control) (Fig. 7B). Finally, the importance of PHF8 HDM activity was demonstrated by the rescue of H4K20me3 levels after overexpression of PHF8 WT, but not of the catalytic mutant (Fig. 7C). Notably, in the case of overexpression of the PHF8 catalytic mutant, an apparent increase in H4K20me3 intensity was observed, further highlighting the importance of the enzymatic activity of PHF8 in preventing heterochromatin mark accumulation during astrocyte differentiation. These data strongly suggest that PHF8 demethylates H4K20me1 at genes crucial for astrocytic differentiation and synapsis formation, such as *Nfia* and *Sparc*, respectively, to facilitate their transcriptional activation. Taken together, our data indicate that the major role of astrocytic PHF8 is to demethylate H4K20me1, preventing ectopic heterochromatin formation during differentiation.

DISCUSSION

Our study reveals an unexpected role of the XLID gene *Phf8* in astrocytes, the most abundant glial cells in the mammalian brain. Our data demonstrated that PHF8 directly regulates the expression of the astrogenic master gene *Nfia* and of genes that are essential for synaptic formation and function (Fig. 7D). Indeed, depletion of astrocytic PHF8 resulted in decreased density and strength of excitatory synapses in neuron-astrocyte co-cultures *in vitro*.

PHF8 targets *Nfia* during astrocyte differentiation

We identified the transcription factor NFIA as a PHF8 transcriptional target (Fig. 7D). The essential role of NFIA in activating the expression of astrocyte-specific genes and facilitating astrocytic differentiation has been extensively reported (Deneen et al., 2006; Piper et al., 2010; Shu et al., 2003). In particular, *in vivo* studies have demonstrated that *Nfia*$^{-/-}$ mice have normal expression of astrocyte markers, but decreased levels of GFAP in the cortex and the hippocampus (das Neves et al., 1999), similar to our observations in PHF8-KD astrocytes *in vitro*. More recent studies have demonstrated that NFIA occupies and regulates the *Gfap* promoter prior to the induction of astrocyte differentiation (Cebolla and Vallejo, 2006; Namihira et al., 2009; Piper et al., 2010). Recently, a study demonstrated that *Nfia* loss in astrocytes leads to diminution of the synaptic function (Huang et al., 2020). Thus, the downregulation of *Nfia* observed in PHF8-depleted astrocytes could be responsible, at least in part, for the phenotype and impaired synaptic transmission of PHF8-KD astrocytes. Furthermore, it has been previously reported that *Nfia* is a Notch target gene (Namihira et al., 2009; Piper et al., 2010). Thus, it is likely that PHF8 regulates *Nfia* expression through the activation of this pathway. We and others (Yatim et al., 2012) demonstrated that PHF8 is a modulator of the Notch signaling pathway. Moreover, we have revealed that *Phf8* is itself a Notch target, suggesting the existence of a regulatory feedback mechanism responsible for *Nfia* transcriptional control, which deserves further studies.

A subpopulation of PHF8 KD astrocytes expresses OLIG2

Upon PHF8 depletion, a subpopulation of astrocytes expressed high levels of OLIG2 markers. Previous studies showed that some astrocytes express OLIG2 in the gray matter of the mouse spinal cord, thalamus and forebrain (Barnabe-Heider et al., 2010; Griemsmann et al., 2015; Guo et al., 2011; Ohayon et al., 2019; Tatsumi et al., 2018). Thus, PHF8 levels might contribute to the redirection of astrocyte subtypes. However, our transcriptomic analysis revealed that PHF8-depleted astrocytes were not enriched in the astrocyte subtypes (A1-A3) expressing OLIG2 (Batiuk et al., 2020), indicating that PHF8 depletion was not involved in the specification of those astrocyte subtypes.

In addition to *Olig2*, we observed the increased expression of another typical oligodendrocyte gene in PHF8-depleted astrocytes: *Plp1*. Given that *Plp1* is not a PHF8 direct target, its transcriptional alteration is probably an indirect consequence of the primary PHF8-induced transcriptional changes. Interestingly, NFIA has also been involved in oligodendrocyte differentiation; thus, its downregulation, resulting from PHF8 loss, might indirectly lead to the upregulation of some oligodendrocyte genes, as we observed from the RNA-seq results.

PHF8 regulates the expression of synaptic genes

In addition to *Nfia*, genes involved in synapse formation were found to be regulated directly by astrocytic PHF8 in our study (Fig. 7D). It is well known that the structural and functional interactions of astrocytes with neurons at synapses are necessary for proper brain function (Araque et al., 2014). In particular, astrocytes participate in synaptic plasticity, i.e. the ability of synapses to strengthen or weaken over time, a key process underlying cognitive performance (Bliss and Collingridge, 1993), by promoting synapse formation or pruning aberrant synapses (Clarke and Barres, 2013; Liddelow and Barres, 2015). PHF8 defects were previously linked to XLID (Koivisto et al., 2007; Loenarz et al., 2010; Qiao et al., 2008), although the underlying mechanism was poorly understood. Previous studies have shown that *Phf8*-KO mice are deficient in learning and memory (Chen et al., 2018) and are resistant to anxiety- and depression-like behaviors (Walsh et al., 2017).

Development (2021) 148, dev194951. doi:10.1242/dev.194951

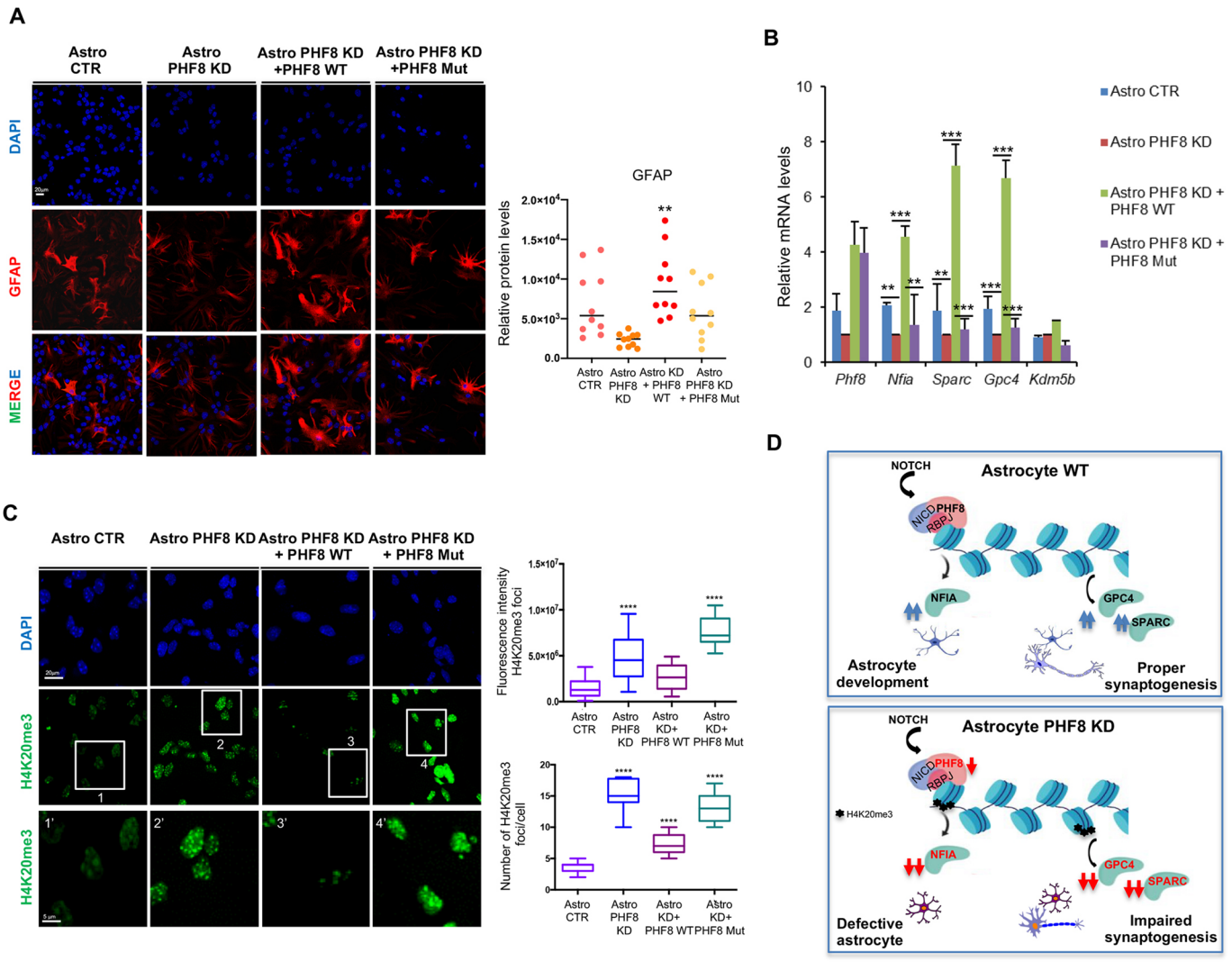

Fig. 7. PHF8 HDM activity is important for astrocyte differentiation. (A) Control and PHF8-depleted NSCs were differentiated to astrocytes over 6 days. Expression of either WT PHF8 or the catalytic mutant (H247A) (Mut) in Astro PHF8-KD was then induced by doxycycline addition and the cells were allowed to differentiate for a further 6 days. The cells were immunostained using GFAP antibody and DAPI (left). The relative protein levels of GFAP per cell were determined using ImageJ (right). $^{**}P<0.01$. (B) WT PHF8 and the catalytic domain were expressed in Astro PHF8-KD and the expression levels of the indicated genes were determined by qPCR. Expression values were normalized to the housekeeping gene *Gapdh*. Values are shown relative to Astro PHF8-KD. *Kdm5b* mRNA was used as a negative control. Data are mean±s.d.; $n=3$ independent biological replicates. $^{**}P<0.01$; $^{***}P<0.001$. (C) WT PHF8 and the catalytic mutant were expressed in Astro PHF8-KD; the levels of H4K20me3 were then established by immunostaining assays. Magnified images show H4K20me3 foci. Images are representative of three biological independent experiments. Fluorescence intensity of H4K20me3 and H4K20me3 foci number were determined using ImageJ. Box plots represent the quantification of the fluorescence intensities and the number of H4K20me3 foci/cell in each population. Boxes show magnified regions below. $^{****}P<0.0001$. (D) Model depicting the contribution of PHF8 to astrocyte differentiation and function. PHF8 directly regulates the expression of the master regulator of astrocyte differentiation *Nfia* as well as genes involved in synapse differentiation and function. Depletion or alteration of PHF8 catalytic activity leads to distinct astrocytes that have deficient synaptic function. Scale bars: 5 µm in C (magnifications); 20 µm in C (main images).

However, only subtle PHF8-mediated transcription changes were observed in neurons and the effects on glial cells were not evaluated. Here, we showed that PHF8 induces profound transcriptional changes in astrocytes, which, in turn, cause important alterations of synaptic transmission *in vitro*. Interestingly, our results demonstrated that synaptic genes are both up- (*Slc1a2* and *Nrxn1*) and downregulated (*Sparc* and *Gpc4*) in PHF8-depleted astrocytes (although downregulated genes showed higher FC values; Fig. S2F) suggesting that PHF8 might be involved in balancing the expression of these genes in astrocytes to regulate synaptic function. Thus, our results suggest that astrocytes might be the main cellular target of PHF8.

PHF8 prevents ectopic heterochromatin formation

Importantly, our study also unveiled the molecular mechanism behind PHF8-mediated transcriptional changes. Our results demonstrated that PHF8 maintains the expression of astrocytic and synaptic genes by maintaining low levels of the H4K20me1 histone mark. PHF8 depletion led to ectopic heterochromatin formation at both global and local levels. Thus, PHF8 HDM activity is crucial for maintenance of the H4K20me1/H4K20me3 equilibrium. Interestingly, the heterochromatic mark H4K20me3 increased, in terms of both its global level and number of foci, upon PHF8 depletion. These data suggest that H4K20me1 is used as a substrate by the histone methyltransferases SUV420H1/2 to

Development (2021) 148, dev194951. doi:10.1242/dev.194951

generate H4K20me3. Consistent with this finding, PHF2, another member of the KDM7 family, limits the accumulation of another heterochromatic mark, H3K9me3, at promoters of cell cycle-related genes in NSCs (Pappa et al., 2019). By contrast, our results demonstrated that depletion of PHF8 led to elevated H4K20me1 levels at the synaptic genes, which correlated with low transcription levels. These results are in agreement with previous studies demonstrating that depletion of PHF8 in neurons resulted in the downregulation of cytoskeleton genes by increasing H4K20me1 levels (Asensio-Juan et al., 2012).

Our work significantly advances current knowledge of the physiological role of PHF8 in astrocyte differentiation and synaptic formation *in vitro*, suggesting that PHF8 may be a key regulator of astrogliogenesis and synaptogenesis. These findings pave the way for the development of pharmacological interventions aimed at improving cognitive function in XLID. Moreover, they prompt us to investigate the contribution of H4K20 methylation not only to neurodevelopmental disorders, but also to other pathological conditions, such as cancer, in which PHF8 is involved. This will increase our understanding of the crosstalk between epigenetics, development and disease.

MATERIALS AND METHODS

Cell culture and differentiation

Mouse NSCs were dissected from cerebral cortices of C57BL/6J mouse fetal brains (E12.5) and cultured in poly-D-lysine (5 µg/ml, 2 h at 37°C)- and laminin (5 µg/ml, 4 h at 37°C)-precoated dishes following previously published procedures (Currle et al., 2007). NSCs were grown in medium containing equal parts of Dulbecco's Modified Eagle Medium/Nutrient Mixture (DMEM F12; without Phenol Red; Thermo Fisher Scientific) and Neurobasal medium (Thermo Fisher Scientific) with penicillin/streptomycin (5%), GlutaMAX (1%), N2 and B27 supplements (Thermo Fisher Scientific), sodium pyruvate (1 mM), nonessential amino acids (0.1 mM), heparin (2 mg/l), HEPES (5 mM), bovine serum albumin (BSA; 25 mg/l) and β-mercaptoethanol (0.01 mM), as previously described (Estaras et al., 2012). Fresh recombinant human epidermal growth factor (EGF) (R&D Systems) and fibroblast growth factor (FGF) (Invitrogen) to final concentrations of 20 ng/ml and 10 ng/ml, respectively, were added to the media. Under these conditions, NSCs maintain the ability to self-renew and to differentiate into a wide range of neural cell types (Currle et al., 2007; Pollard et al., 2006).

For NSC differentiation into astrocytes, the medium was replaced with a differentiation medium (astrocytic medium) containing DMEM/F-12, 5% N2, GlutaMAX and 10% fetal bovine serum (FBS); fresh astrocytic medium was supplied every 2 days.

Human HEK 293T cells were maintained in culture under standard conditions (Blanco-Garcia et al., 2009), cultured in DMEM supplemented with 10% FBS.

Astrocyte-neuron co-cultures

Primary neuronal cultures were obtained from the hippocampus of 18-day-old fetal C57BL/6 wild-type mice (Charles River). Briefly, dissociated cells were plated onto previously differentiated astrocytes (10 days) in 12-well multiwell plates at a seeding density of 0.3×10^6 and maintained in Neurobasal medium supplemented with 2% B27 (Life Technologies), penicillin/streptomycin (1%), L-glutamine (0.5 mM) and glutamate (12 µM). Cultures were maintained in standard conditions at 37°C and 5% CO_2. After 3 days *in vitro*, the medium was partially replaced by fresh medium.

Antibodies and reagents

The antibodies and reagents used were: anti-PHF8 (Abcam, ab36068; western blot 1:1000; ChIP 1:500; immunochemistry 1:500), anti-H4K20me1 (Abcam, ab9051 ChIP 2 µg/ml; immunochemistry 1:500), anti-H4K20me3 (Abcam, ab9053; ChIP 2 µg/ml; immunochemistry 1:500), anti-H3K9me2 (Abcam, ab1220; ChIP 2 µg/ml; immunochemistry 1:500), anti-H3K27me3 (Millipore, 07449; 1:500), H3K4me3 (Abcam, ab8580; 1:500), anti-GAPDH (Synaptic Systems, 247002; 1:500), anti-β-tubulin 3 (TUJ1; BioLegend, MMS-435P; 1:500), anti-GFAP (Agilent Dako, z0334, and Synaptic Systems, 173 004; 1:500), anti-nestin (Abcam, ab5968; 1:500), anti-OLIG2 (Merck, AB9610; 1:500), anti-alpha-tubulin (Abcam, ab4074; 1:10,000), anti-GLAST (Abcam, ab416; 1:500), anti-aquaporin 4 (Abcam, ab125049; 1:500), anti-EAAT2 (Abcam, ab41621; 1:500), anti-NG2 chondroitin sulfate proteoglycan (Merck, AB5320; 1:500), anti-GPR17 (Cayman Chemical, 10136; 1:500), anti-IBA-1 (Thermo Fisher Scientific, PA5-27436; 1:500), anti-bassoon (Synaptic Systems, 141004; 1:500), anti-SHANK2 (Synaptic Systems, 162202; 1:500), anti-SHANK3 (Synaptic Systems, 162304; 1:500) and DAPI (Thermo Fisher Scientific , D1306).

Plasmids and recombinant proteins

Previously published specific lentiviral vectors were either purchased from Sigma-Aldrich or cloned in the pLKO.1-puro vector (Sigma-Aldrich) using the AgeI and EcoRI sites (brackets indicate the target sequence): pLKO-random (CAACAAGATGAAGAGCACC) and pLKO-mPHF8_1 (GCAGGTAAATGGGAGAGGTT). PHF8 human cDNA from pEF6-HA-PHF8 (kindly provided by Dr C. Leonarz (Institute of Pharmaceutical Sciences, University of Freiburg, Germany) was cloned into the pINDUCER vector (#44012, Addgene) between the attB1 and attB2 sites. Both PHF8 WT and catalytic mutant H247A were induced upon doxycycline addition (1 µg/ml). pCIG-FLAG-SMAD3-S/D, BMP4 and BMP7 were kindly provided by Dr Elisa Martí (IBMB, CSIC, Barcelona, Spain). Primer sequences are described in Table S1.

Lentiviral transduction

Lentiviral transduction was carried out as previously described (Asensio-Juan et al., 2017). Briefly, HEK 293T cells were transfected with a mix of packaging, envelop and shRNA transfer vector DNAs (6, 5 and 7 µg, respectively). The medium was collected 24-30 h later and the virus concentrated by ultracentrifugation [26,000 rpm (121.139 ***g***), 2 h at 4°C]. Viral particles were then used to transduce NSCs. After 24 h, cells were selected with either puromycin (2 µg/ml; Merck, P8833) (pLKO.1 vectors) or geneticine (600 µg/ml; Merck, 345810) (pINDUCER vectors). After selection, 99-100% of the cells expressed the shRNA.

ChIP assays

ChIP assays were performed as previously described (Valls et al., 2007) with modifications: 10^6 NSCs were fixed with formaldehyde (1%) for 10 min. Fixation was stopped by adding 0.125 mM glycine. Cells were lysed in lysis buffer (1% SDS; 10 mM EDTA, pH 8.0; 50 mM Tris-HCl, pH 8.1). Chromatin fragmentation was performed in a Bioruptor sonicator (Diagenode) before immunoprecipitation. The immunocomplex was captured using Magna ChIP Protein A Magnetic Beads (Millipore). After decrosslinking, DNA was purified by ethanol precipitation. ChIP DNA was quantified by qPCR with SYBR Green (Roche) in a LightCycler 480 PCR system (Roche) using the primers indicated in Table S1. The input percentage was used for quantification of the immunoprecipitated material with respect to the starting chromatin. Integrative Genomics Viewer (IGV) (https://software.broadinstitute.org/software/igv/) was used to visualize a particular region.

Indirect immunofluorescence and quantification

Immunofluorescence assays were performed as previously described (Sanchez-Molina et al., 2014). Cells were fixed for 20 min in 4% paraformaldehyde and permeabilized with PBS-Triton X-100 (0.1%) before blocking at room temperature for 1 h in 1% BSA (in PBS with 0.1% Triton X-100). Primary antibodies were used overnight at 4°C. Finally, cells were incubated for 2 h at room temperature with Alexa-conjugated secondary antibodies and DAPI (0.1 ng/µl) (Sigma-Aldrich). Images were captured using a Leica SP5 confocal microscope with LAS-AF software. Two different methods of quantification were performed depending on the experiment. In the case of histone marks and PHF8 immunostaining, the

Development (2021) 148, dev194951. doi:10.1242/dev.194951

fluorescence intensity per cell was measured using ImageJ and the corrected cell fluorescence was calculated using the formula: integrated density−(area of selected cell×mean fluorescence of background readings).

For H4K20me3, the number of foci per cell was also calculated. Finally, the percentage of positive cells per field was determined for the cell-lineage markers nestin, GLAST, GFAP, TUBβ3 and OLIG2. The maximum and minimum cell body diameters of neurons were measured on immunofluorescence confocal images of co-cultures with PHF8-KD or CTR astrocytes, fixed and stained for TUBβ3 and DAPI, using the straight-line tool of ImageJ software followed by the Analyze>Measure command. Neuronal cell density was evaluated in the same images by counting the number of neuronal cell bodies in the acquired area. The quantification for the co-culture experiments was performed as indicated above.

RNA extraction and qPCR

TRIzol reagent (Invitrogen) was used to extract RNA following the manufacturer's instructions. Reverse transcription was performed with 2 µg of RNA using High Capacity cDNA Reverse Transcription Kit (Thermo Fisher Scientific) and qPCR was performed with SYBR Green (Roche) in a LightCycler 480 (Roche). Specific primer pairs are detailed in Table S1.

Western blot

Immunoblotting was performed using standard procedures (Towbin et al., 1979) and visualized by means of an ECL kit (Merck, GERPN2106)

MACS isolation of astrocyte

Purified astrocytes were isolated from E18 embryos or P2 or P7 mouse whole brains by MACS (Miltenyi Biotec) with anti-GLAST (ACSA 2) MicroBeads according to the manufacturer's instructions. Cells were lysed with a buffer containing 1% SDS, 2 mM EDTA pH 7.4, 10 mM Tris-HCl pH 7.4 and protease inhibitor (1:100; Merck, P8340).

ChIP-seq

ChIP was carried out as previously described (Fueyo et al., 2018) with minor modifications, described as follows. The sonication step was performed in a Bioruptor sonicator. The input sample, corresponding to the 10% of the total material, was reserved at this point. The PHF8 antibody (Abcam, ab36068) used for immunoprecipitation was the same as that used in the ChIP assays described above. After decrosslinking, DNA was purified by ethanol precipitation. The libraries were prepared and sequenced in a HiSeq 2000 Sequencing System (Illumina) (Table S2). In total, 50 base pairs sequences were mapped using Bowtie2 (Langmead and Salzberg, 2012) to the *Mus musculus* genome release 10 (mm10); files were filtered to remove duplicates and peaks were called using MACS (Zhang et al., 2008) and an effective genome size of 1.87 Gb and a *P*-value of 0.001 for PHF8 ChIP-seq. The Bioconductor package ChIPseeker (Yu et al., 2015) was used to annotate the genes of each peak. Specifically, the function annotatePeak matches peaks with genomic features extracted from mm10 (UCSC) and calculates the proportion of peaks matching each feature. Homer tool (http://homer.ucsd.edu/homer/motif/) was used to identify DNA-bindig motif enrichment. For further details, see Table S2. ChIP-seq data have been deposited in the GEO database under the accession GSE141969.

RNA-seq

RNA was extracted using High Pure RNA Isolation Kit (Roche) followed by DNaseI treatment from two biological independent samples. Libraries were prepared using the TruSeq Stranded Total RNA Sample Preparation Kit with Ribo-Zero Human/Mouse/Rat Kit (Illumina) according to the manufacturer's protocol. Briefly, 500 ng of total RNA was used for ribosomal RNA (rRNA) depletion. Then, rRNA-depleted RNA was fragmented for 4.5 min. The remaining steps of the library preparation were followed according to the manufacturer's instructions. Final libraries were analyzed using the Agilent DNA 1000 Kit to estimate the quantity and check the size distribution, and were then quantified by qPCR using the KAPA Library Quantification Kit (Roche) prior to amplification with cBot (Illumina). The libraries were sequenced on Illumina High HiSeq 2500 Sequencing System with paired-end 50 base pair-long reads (Table S2). Alignment was performed using STAR (Dobin et al., 2013); aligned reads were assigned to genes using HTSeq (Anders et al., 2015) and differential expression analysis was performed using DESeq2 (Love et al., 2014). RNA-seq data have been deposited in the GEO database under the accession GSE141970.

Analysis of synapses

The percentage of synapses with pre- and postsynaptic terminals was determined in a single confocal plane using ImageJ software. Regions of interest (ROIs) were drawn using the freehand line tool on TUBβ3 images and the length of the segments was measured using the analyze function. Bassoon, SHANK2 and double-positive puncta were counted by generating merge images of bassoon/SHANK2/TUBβ3. Synapse density was calculated dividing the number of puncta by the ROI length, which corresponds to the dendrite length.

Electrophysiology

Whole-cell voltage clamp recordings were performed using a MultiClamp 700A amplifier (Molecular Devices), a 1320A Digidata (Molecular Devices), coupled to pCLAMP 10 Software (Molecular Devices) and an inverted Axiovert 200 microscope (Zeiss). mEPSCs were recorded from DIV 12-14 neurons in Krebs-Ringer's HEPES solution (KRH) (125 mM NaCl, 5 mM KCl, 1.2 mM $MgSO_4$, 1.2 mM KH_2PO, 2 mM $CaCl_2$, 6 mM D-glucose and 25 mM HEPES/NaOH, pH 7.4), supplemented with 1 µM tetrodotoxin (Abcam, ab120055) and 20 µM bicuculline (Abcam, ab120110). Experiments were performed at room temperature (20-25°C), setting the holding potential at −70 mV and using the following internal solution: (130 mM potassium gluconate, 10 mM KCl, 1 mM EGTA, 10 mM HEPES, 2 mM $MgCl_2$, 4 mM MgATP, 0.3 mM Tris-GTP; pH 7.4, adjusted with KOH). Recording pipettes were pulled from patch-clamp borosilicate capillary glass (World Precision Instruments) to a tip resistance of 3-5 MΩ using a two-stage vertical puller (Narishige). Traces were sampled at 10 kHz and filtered at 2 kHz. Series resistance was monitored during recording. mEPSCs were detected offline using Clampfit software (Molecular Devices) setting a threshold of 7 pA.

Resting membrane potential was evaluated immediately after breaking the cell-attached patch, by setting the amplifier to zero current mode (I=0).

Statistical analysis

Quantitative data were expressed as mean±standard deviation (s.d.). The Mann–Whitney Rank Sum Test was used to quantify the frequency and amplitude of the excitatory postsynaptic currents. The Jaccard index was used to determine the similarity between the samples; it measures the similarity between two nominal attributes by taking the intersection of both and dividing it by their union (Vorontsov et al., 2013). The significance of differences between two groups was assessed using the Student's *t*-test; two-way ANOVAs were used for three or more groups and the relative viabilities were compared using Tukey's multiple comparisons test (*P<0.05, **P<0.01, ***P<0.001, ****P<0.0001).

Acknowledgements

We would like to thank Dr Christoph Loenarz for the HA-PHF8 vector; Drs A. Jordá, F. Azorín, J. Bernues, G. Vicent, A. Vaquero and E. Martí for reagents; M. Arbonés and M. J. Barallobre for advice; and team members for helpful comments and suggestions.

Competing interests

The authors declare no competing or financial interests.

Author contributions

Conceptualization: S.I., C.V., M.A.M.-B.; Methodology: S.I., N.P., M.G., C.N., M.L., C.V., X.C., M.A.M.-B.; Software: N.P., X.C.; Validation: S.I., M.V.-M.; Formal analysis: N.P., X.C.; Investigation: S.I., M.G., C.N., M.L.; Resources: C.V., M.A.M.-B.; Data curation: M.G., X.C., M.A.M.-B.; Writing - original draft: M.A.M.-B.; Writing - review & editing: S.I., N.P., C.V., X.C.; Supervision: M.A.M.-B.; Project administration: M.A.M.-B.; Funding acquisition: C.V., M.A.M.-B, X.C.

Funding
This study was supported by grants from the Spanish Ministry of Economy (Ministerio de Economía, Industria y Competitividad, Gobierno de España; BFU2015-69248-P and PGC2018-096082-B-I00 to M.A.M.-B.) and Ministerio de Ciencia e Innovación (PID2019-111217RB-I00 to X.C) and a Travelling Fellowship from Boehringer Ingelheim to S.I. Open access funding provided by Consejo Superior de Investigaciones Científicas. Deposited in PMC for immediate release.

Data availability
ChIP-seq data have been deposited in the Gene Expression database under accession number GSE141969. RNA-seq data have been deposited in the Gene Expression Omnibus database under accession number GSE141970.

Peer review history
The peer review history is available online at https://journals.biologists.com/dev/article-lookup/doi/10.1242/dev.194951

References

Abidi, F. E., Miano, M. G., Murray, J. C. and Schwartz, C. E. (2007). A novel mutation in the PHF8 gene is associated with X-linked mental retardation with cleft lip/cleft palate. *Clin. Genet.* **72**, 19-22. doi:10.1111/j.1399-0004.2007.00817.x
Anders, S., Pyl, P. T. and Huber, W. (2015). HTSeq–a Python framework to work with high-throughput sequencing data. *Bioinformatics* **31**, 166-169. doi:10.1093/bioinformatics/btu638
Araque, A., Carmignoto, G., Haydon, P. G., Oliet, S. H. R., Robitaille, R. and Volterra, A. (2014). Gliotransmitters travel in time and space. *Neuron* **81**, 728-739. doi:10.1016/j.neuron.2014.02.007
Asensio-Juan, E., Gallego, C. and Martínez-Balbás, M. A. (2012). The histone demethylase PHF8 is essential for cytoskeleton dynamics. *Nucleic Acids Res.* **40**, 9429-9440. doi:10.1093/nar/gks716
Asensio-Juan, E., Fueyo, R., Pappa, S., Iacobucci, S., Badosa, C., Lois, S., Balada, M., Bosch-Presegué, L., Vaquero, A., Gutiérrez, S. et al. (2017). The histone demethylase PHF8 is a molecular safeguard of the IFNγ response. *Nucleic Acids Res.* **45**, 3800-3811. doi:10.1093/nar/gkw1346
Barnabé-Heider, F., Göritz, C., Sabelström, H., Takebayashi, H., Pfrieger, F. W., Meletis, K. and Frisén, J. (2010). Origin of new glial cells in intact and injured adult spinal cord. *Cell Stem Cell* **7**, 470-482. doi:10.1016/j.stem.2010.07.014
Batiuk, M. Y., Martirosyan, A., Wahis, J., de Vin, F., Marneffe, C., Kusserow, C., Koeppen, J., Viana, J. F., Oliveira, J. F., Voet, T. et al. (2020). Identification of region-specific astrocyte subtypes at single cell resolution. *Nat. Commun.* **11**, 1220. doi:10.1038/s41467-019-14198-8
Blanco-García, N., Asensio-Juan, E., de la Cruz, X. and Martínez-Balbás, M. A. (2009). Autoacetylation regulates P/CAF nuclear localization. *J. Biol. Chem.* **284**, 1343-1352. doi:10.1074/jbc.M806075200
Bliss, T. V. P. and Collingridge, G. L. (1993). A synaptic model of memory: long-term potentiation in the hippocampus. *Nature* **361**, 31-39. doi:10.1038/361031a0
Cebolla, B. and Vallejo, M. (2006). Nuclear factor-I regulates glial fibrillary acidic protein gene expression in astrocytes differentiated from cortical precursor cells. *J. Neurochem.* **97**, 1057-1070. doi:10.1111/j.1471-4159.2006.03804.x
Chelly, J., Khelfaoui, M., Francis, F., Chérif, B. and Bienvenu, T. (2006). Genetics and pathophysiology of mental retardation. *Eur. J. Hum. Genet.* **14**, 701-713. doi:10.1038/sj.ejhg.5201595
Chen, X., Wang, S., Zhou, Y., Han, Y., Li, S., Xu, Q., Xu, L., Zhu, Z., Deng, Y., Yu, L. et al. (2018). Phf8 histone demethylase deficiency causes cognitive impairments through the mTOR pathway. *Nat. Commun.* **9**, 114. doi:10.1038/s41467-017-02531-y
Cheng, C., Lau, S. K. M. and Doering, L. C. (2016). Astrocyte-secreted thrombospondin-1 modulates synapse and spine defects in the fragile X mouse model. *Mol. Brain* **9**, 74. doi:10.1186/s13041-016-0256-9
Clarke, L. E. and Barres, B. A. (2013). Emerging roles of astrocytes in neural circuit development. *Nat. Rev. Neurosci.* **14**, 311-321. doi:10.1038/nrn3484
Cresto, N., Pillet, L. E., Billuart, P. and Rouach, N. (2019). Do astrocytes play a role in intellectual disabilities? *Trends Neurosci.* **42**, 518-527. doi:10.1016/j.tins.2019.05.011
Currle, D. S., Hu, J. S., Kolski-Andreaco, A. and Monuki, E. S. (2007). Culture of mouse neural stem cell precursors. *J. Vis. Exp.* **2**, e152. doi:10.3791/152
das Neves, L., Duchala, C. S., Godinho, F., Haxhiu, M. A., Colmenares, C., Macklin, W. B., Campbell, C. E., Butz, K. G. and Gronostajski, R. M. (1999). Disruption of the murine nuclear factor I-A gene (Nfia) results in perinatal lethality, hydrocephalus, and agenesis of the corpus callosum. *Proc. Natl. Acad. Sci. USA* **96**, 11946-11951. doi:10.1073/pnas.96.21.11946
Deneen, B., Ho, R., Lukaszewicz, A., Hochstim, C. J., Gronostajski, R. M. and Anderson, D. J. (2006). The transcription factor NFIA controls the onset of gliogenesis in the developing spinal cord. *Neuron* **52**, 953-968. doi:10.1016/j.neuron.2006.11.019
Dobin, A., Davis, C. A., Schlesinger, F., Drenkow, J., Zaleski, C., Jha, S., Batut, P., Chaisson, M. and Gingeras, T. R. (2013). STAR: ultrafast universal RNA-seq aligner. *Bioinformatics* **29**, 15-21. doi:10.1093/bioinformatics/bts635
ENCODE Project Consortium (2012). An integrated encyclopedia of DNA elements in the human genome. *Nature* **489**, 57-74. doi:10.1038/nature11247
Estaras, C., Akizu, N., Garcia, A., Beltran, S., de la Cruz, X. and Martinez-Balbas, M. A. (2012). Genome-wide analysis reveals that Smad3 and JMJD3 HDM co-activate the neural developmental program. *Development* **139**, 2681-2691. doi:10.1242/dev.078345
Farhy-Tselnicker, I., van Casteren, A. C. M., Lee, A., Chang, V. T., Aricescu, A. R. and Allen, N. J. (2017). Astrocyte-Secreted Glypican 4 regulates release of neuronal Pentraxin 1 from Axons to induce functional synapse formation. *Neuron* **96**, 428-445.e13. doi:10.1016/j.neuron.2017.09.053
Fortschegger, K. and Shiekhattar, R. (2011). Plant homeodomain fingers form a helping hand for transcription. *Epigenetics* **6**, 4-8. doi:10.4161/epi.6.1.13297
Fortschegger, K., de Graaf, P., Outchkourov, N. S., van Schaik, F. M. A., Timmers, H. T. M. and Shiekhattar, R. (2010). PHF8 targets histone methylation and RNA polymerase II to activate transcription. *Mol. Cell. Biol.* **30**, 3286-3298. doi:10.1128/MCB.01520-09
Fueyo, R., Iacobucci, S., Pappa, S., Estarás, C., Lois, S., Vicioso-Mantis, M., Navarro, C., Cruz-Molina, S., Reyes, J. C., Rada-Iglesias, Á. et al. (2018). Lineage specific transcription factors and epigenetic regulators mediate TGFβ-dependent enhancer activation. *Nucleic Acids Res.* **46**, 3351-3365. doi:10.1093/nar/gky093
Ge, W., Martinowich, K., Wu, X., He, F., Miyamoto, A., Fan, G., Weinmaster, G. and Sun, Y. E. (2002). Notch signaling promotes astrogliogenesis via direct CSL-mediated glial gene activation. *J. Neurosci. Res.* **69**, 848-860. doi:10.1002/jnr.10364
Griemsmann, S., Höft, S. P., Bedner, P., Zhang, J., von Staden, E., Beinhauer, A., Degen, J., Dublin, P., Cope, D. W., Richter, N. et al. (2015). Characterization of Panglial Gap junction networks in the thalamus, neocortex, and hippocampus reveals a unique population of glial cells. *Cereb. Cortex* **25**, 3420-3433. doi:10.1093/cercor/bhu157
Guo, F., Maeda, Y., Ma, J., Delgado, M., Sohn, J., Miers, L., Ko, E. M., Bannerman, P., Xu, J., Wang, Y. et al. (2011). Macroglial plasticity and the origins of reactive astroglia in experimental autoimmune encephalomyelitis. *J. Neurosci.* **31**, 11914-11928. doi:10.1523/JNEUROSCI.1759-11.2011
Hillen, A. E. J., Burbach, J. P. H. and Hol, E. M. (2018). Cell adhesion and matricellular support by astrocytes of the tripartite synapse. *Prog. Neurobiol.* **165-167**, 66-86. doi:10.1016/j.pneurobio.2018.02.002
Horton, J. R., Upadhyay, A. K., Qi, H. H., Zhang, X., Shi, Y. and Cheng, X. (2010). Enzymatic and structural insights for substrate specificity of a family of jumonji histone lysine demethylases. *Nat. Struct. Mol. Biol.* **17**, 38-43. doi:10.1038/nsmb.1753
Huang, A. Y.-S., Woo, J., Sardar, D., Lozzi, B., Bosquez Huerta, N. A., Lin, C.-C. J., Felice, D., Jain, A., Paulucci-Holthauzen, A. and Deneen, B. (2020). Region-specific transcriptional control of astrocyte function oversees local circuit activities. *Neuron* **106**, 992-1008.e9. doi:10.1016/j.neuron.2020.03.025
Jori, F. P., Galderisi, U., Napolitano, M. A., Cipollaro, M., Cascino, A., Giordano, A. and Melone, M. A. B. (2007). RB and RB2/P130 genes cooperate with extrinsic signals to promote differentiation of rat neural stem cells. *Mol. Cell. Neurosci.* **34**, 299-309. doi:10.1016/j.mcn.2006.11.009
Kleine-Kohlbrecher, D., Christensen, J., Vandamme, J., Abarrategui, I., Bak, M., Tommerup, N., Shi, X., Gozani, O., Rappsilber, J., Salcini, A. E. et al. (2010). A functional link between the histone demethylase PHF8 and the transcription factor ZNF711 in X-linked mental retardation. *Mol. Cell* **38**, 165-178. doi:10.1016/j.molcel.2010.03.002
Koivisto, A. M., Ala-Mello, S., Lemmelä, S., Komu, H. A., Rautio, J. and Järvelä, I. (2007). Screening of mutations in the PHF8 gene and identification of a novel mutation in a Finnish family with XLMR and cleft lip/cleft palate. *Clin. Genet.* **72**, 145-149. doi:10.1111/j.1399-0004.2007.00836.x
Kramer, J. M. and van Bokhoven, H. (2009). Genetic and epigenetic defects in mental retardation. *Int. J. Biochem. Cell Biol.* **41**, 96-107. doi:10.1016/j.biocel.2008.08.009
Kucukdereli, H., Allen, N. J., Lee, A. T., Feng, A., Ozlu, M. I., Conatser, L. M., Chakraborty, C., Workman, G., Weaver, M., Sage, E. H. et al. (2011). Control of excitatory CNS synaptogenesis by astrocyte-secreted proteins Hevin and SPARC. *Proc. Natl. Acad. Sci. USA* **108**, E440-E449. doi:10.1073/pnas.1104977108
Langmead, B. and Salzberg, S. L. (2012). Fast gapped-read alignment with Bowtie 2. *Nat. Methods* **9**, 357-359. doi:10.1038/nmeth.1923
Laumonnier, F., Holbert, S., Ronce, N., Faravelli, F., Lenzner, S., Schwartz, C. E., Lespinasse, J., Van Esch, H., Lacombe, D., Goizet, C. et al. (2005). Mutations in PHF8 are associated with X linked mental retardation and cleft lip/cleft palate. *J. Med. Genet.* **42**, 780-786. doi:10.1136/jmg.2004.029439
Li, H., Ilin, S., Wang, W., Duncan, E. M., Wysocka, J., Allis, C. D. and Patel, D. J. (2006). Molecular basis for site-specific read-out of histone H3K4me3 by the BPTF PHD finger of NURF. *Nature* **442**, 91-95. doi:10.1038/nature04802
Liddelow, S. and Barres, B. (2015). SnapShot: astrocytes in health and disease. *Cell* **162**, 1170-1170.e1. doi:10.1016/j.cell.2015.08.029
Liu, W., Tanasa, B., Tyurina, O. V., Zhou, T. Y., Gassmann, R., Liu, W. T., Ohgi, K. A., Benner, C., Garcia-Bassets, I., Aggarwal, A. K. et al. (2010). PHF8

mediates histone H4 lysine 20 demethylation events involved in cell cycle progression. *Nature* **466**, 508-512. doi:10.1038/nature09272

Loenarz, C., Ge, W., Coleman, M. L., Rose, N. R., Cooper, C. D. O., Klose, R. J., Ratcliffe, P. J. and Schofield, C. J. (2010). PHF8, a gene associated with cleft lip/palate and mental retardation, encodes for an N^{ε}-dimethyl lysine demethylase. *Hum. Mol. Genet.* **19**, 217-222. doi:10.1093/hmg/ddp480

Love, M. I., Huber, W. and Anders, S. (2014). Moderated estimation of fold change and dispersion for RNA-seq data with DESeq2. *Genome Biol.* **15**, 550. doi:10.1186/s13059-014-0550-8

Martini, S., Bernoth, K., Main, H., Ortega, G. D., Lendahl, U., Just, U. and Schwanbeck, R. (2013). A critical role for Sox9 in notch-induced astrogliogenesis and stem cell maintenance. *Stem Cells* **31**, 741-751. doi:10.1002/stem.1320

McGann, J. C., Lioy, D. T. and Mandel, G. (2012). Astrocytes conspire with neurons during progression of neurological disease. *Curr. Opin. Neurobiol.* **22**, 850-858. doi:10.1016/j.conb.2012.03.009

Namihira, M., Kohyama, J., Semi, K., Sanosaka, T., Deneen, B., Taga, T. and Nakashima, K. (2009). Committed neuronal precursors confer astrocytic potential on residual neural precursor cells. *Dev. Cell* **16**, 245-255. doi:10.1016/j.devcel.2008.12.014

Ohayon, D., Escalas, N., Cochard, P., Glise, B., Danesin, C. and Soula, C. (2019). Sulfatase 2 promotes generation of a spinal cord astrocyte subtype that stands out through the expression of Olig2. *Glia* **67**, 1478-1495. doi:10.1002/glia.23621

Pappa, S., Padilla, N., Iacobucci, S., Vicioso, M., Álvarez de la Campa, E., Navarro, C., Marcos, E., de la Cruz, X. and Martínez-Balbás, M. A. (2019). PHF2 histone demethylase prevents DNA damage and genome instability by controlling cell cycle progression of neural progenitors. *Proc. Natl. Acad. Sci. USA* **116**, 19464-19473. doi:10.1073/pnas.1903188116

Piper, M., Barry, G., Hawkins, J., Mason, S., Lindwall, C., Little, E., Sarkar, A., Smith, A. G., Moldrich, R. X., Boyle, G. M. et al. (2010). NFIA controls telencephalic progenitor cell differentiation through repression of the Notch effector Hes1. *J. Neurosci.* **30**, 9127-9139. doi:10.1523/JNEUROSCI.6167-09.2010

Pollard, S. M., Conti, L., Sun, Y., Goffredo, D. and Smith, A. (2006). Adherent neural stem (NS) cells from fetal and adult forebrain. *Cereb. Cortex* **16** Suppl. 1, i112-i120. doi:10.1093/cercor/bhj167

Qi, H. H., Sarkissian, M., Hu, G.-Q., Wang, Z., Bhattacharjee, A., Gordon, D. B., Gonzales, M., Lan, F., Ongusaha, P. P., Huarte, M. et al. (2010). Histone H4K20/H3K9 demethylase PHF8 regulates zebrafish brain and craniofacial development. *Nature* **466**, 503-507. doi:10.1038/nature09261

Qiao, Y., Liu, X., Harvard, C., Hildebrand, M. J., Rajcan-Separovic, E., Holden, J. J. A. and Lewis, M. E. S. (2008). Autism-associated familial microdeletion of Xp11.22. *Clin. Genet.* **74**, 134-144. doi:10.1111/j.1399-0004.2008.01028.x

Qiu, J., Shi, G., Jia, Y., Li, J., Wu, M., Dong, S. and Wong, J. (2010). The X-linked mental retardation gene PHF8 is a histone demethylase involved in neuronal differentiation. *Cell Res.* **20**, 908-918. doi:10.1038/cr.2010.81

Ropers, H.-H. and Hamel, B. C. J. (2005). X-linked mental retardation. *Nat. Rev. Genet.* **6**, 46-57. doi:10.1038/nrg1501

Sánchez-Molina, S., Estarás, C., Oliva, J. L., Akizu, N., Asensio-Juan, E., Rojas, J. M. and Martínez-Balbás, M. A. (2014). Regulation of CBP and Tip60 coordinates histone acetylation at local and global levels during Ras-induced transformation. *Carcinogenesis* **35**, 2194-2202. doi:10.1093/carcin/bgu111

Shu, T., Butz, K. G., Plachez, C., Gronostajski, R. M. and Richards, L. J. (2003). Abnormal development of forebrain midline glia and commissural projections in *Nfia* knock-out mice. *J. Neurosci.* **23**, 203-212. doi:10.1523/JNEUROSCI.23-01-00203.2003

Siderius, L. E., Hamel, B. C. J., van Bokhoven, H., de Jager, F., van den Helm, B., Kremer, H., Heineman-de Boer, J. A., Ropers, H.-H. and Mariman, E. C. M. (1999). X-linked mental retardation associated with cleft lip/palate maps to Xp11.3-q21.3. *Am. J. Med. Genet.* **85**, 216-220. doi:10.1002/(SICI)1096-8628(19990730)85:3<216::AID-AJMG6>3.0.CO;2-X

Singh, S. K., Stogsdill, J. A., Pulimood, N. S., Dingsdale, H., Kim, Y. H., Pilaz, L.-J., Kim, I. H., Manhaes, A. C., Rodrigues, W. S., Jr., Pamukcu, A. et al. (2016). Astrocytes assemble Thalamocortical Synapses by Bridging NRX1α and NL1 via Hevin. *Cell* **164**, 183-196. doi:10.1016/j.cell.2015.11.034

Sun, Y., Nadal-Vicens, M., Misono, S., Lin, M. Z., Zubiaga, A., Hua, X., Fan, G. and Greenberg, M. E. (2001). Neurogenin promotes neurogenesis and inhibits glial differentiation by independent mechanisms. *Cell* **104**, 365-376. doi:10.1016/S0092-8674(01)00224-0

Tatsumi, K., Isonishi, A., Yamasaki, M., Kawabe, Y., Morita-Takemura, S., Nakahara, K., Terada, Y., Shinjo, T., Okuda, H., Tanaka, T. et al. (2018). Olig2-Lineage astrocytes: a distinct subtype of astrocytes that differs from GFAP astrocytes. *Front. Neuroanat.* **12**, 8. doi:10.3389/fnana.2018.00008

Towbin, H., Staehelin, T. and Gordon, J. (1979). Electrophoretic transfer of proteins from polyacrylamide gels to nitrocellulose sheets: procedure and some applications. *Proc. Natl. Acad. Sci. USA* **76**, 4350-4354.

Tsukada, Y.-i., Ishitani, T. and Nakayama, K. I. (2010). KDM7 is a dual demethylase for histone H3 Lys 9 and Lys 27 and functions in brain development. *Genes Dev.* **24**, 432-437. doi:10.1101/gad.1864410

Valls, E., Blanco-Garcia, N., Aquizu, N., Piedra, D., Estaras, C., de la Cruz, X. and Martinez-Balbas, M. A. (2007). Involvement of chromatin and histone deacetylation in SV40 T antigen transcription regulation. *Nucleic Acids Res.* **35**, 1958-1968. doi:10.1093/nar/gkl1113

Vorontsov, I. E., Kulakovskiy, I. V. and Makeev, V. J. (2013). Jaccard index based similarity measure to compare transcription factor binding site models. *Algorithms Mol. Biol.* **8**, 23. doi:10.1186/1748-7188-8-23

Walsh, R. M., Shen, E. Y., Bagot, R. C., Anselmo, A., Jiang, Y., Javidfar, B., Wojtkiewicz, G. J., Cloutier, J., Chen, J. W., Sadreyev, R. et al. (2017). Phf8 loss confers resistance to depression-like and anxiety-like behaviors in mice. *Nat. Commun.* **8**, 15142. doi:10.1038/ncomms15142

Wen, H., Li, J., Song, T., Lu, M., Kan, P.-Y., Lee, M. G., Sha, B. and Shi, X. (2010). Recognition of histone H3K4 trimethylation by the plant homeodomain of PHF2 modulates histone demethylation. *J. Biol. Chem.* **285**, 9322-9326. doi:10.1074/jbc.C109.097667

Yatim, A., Benne, C., Sobhian, B., Laurent-Chabalier, S., Deas, O., Judde, J.-G., Lelievre, J.-D., Levy, Y. and Benkirane, M. (2012). NOTCH1 nuclear interactome reveals key regulators of its transcriptional activity and oncogenic function. *Mol. Cell* **48**, 445-458. doi:10.1016/j.molcel.2012.08.022

Yu, G., Wang, L.-G. and He, Q.-Y. (2015). ChIPseeker: an R/Bioconductor package for ChIP peak annotation, comparison and visualization. *Bioinformatics* **31**, 2382-2383. doi:10.1093/bioinformatics/btv145

Zhang, Y., Liu, T., Meyer, C. A., Eeckhoute, J., Johnson, D. S., Bernstein, B. E., Nusbaum, C., Myers, R. M., Brown, M., Li, W. et al. (2008). Model-based analysis of ChIP-Seq (MACS). *Genome Biol.* **9**, R137. doi:10.1186/gb-2008-9-9-r137

Zhang, Y., Chen, K., Sloan, S. A., Bennett, M. L., Scholze, A. R., O'Keeffe, S., Phatnani, H. P., Guarnieri, P., Caneda, C., Ruderisch, N. et al. (2014). An RNA-sequencing transcriptome and splicing database of glia, neurons, and vascular cells of the cerebral cortex. *J. Neurosci.* **34**, 11929-11947. doi:10.1523/JNEUROSCI.1860-14.2014

Zhang, Y., Sloan, S. A., Clarke, L. E., Caneda, C., Plaza, C. A., Blumenthal, P. D., Vogel, H., Steinberg, G. K., Edwards, M. S. B., Li, G. et al. (2016). Purification and characterization of progenitor and mature human astrocytes reveals transcriptional and functional differences with mouse. *Neuron* **89**, 37-53. doi:10.1016/j.neuron.2015.11.013

Figure S1

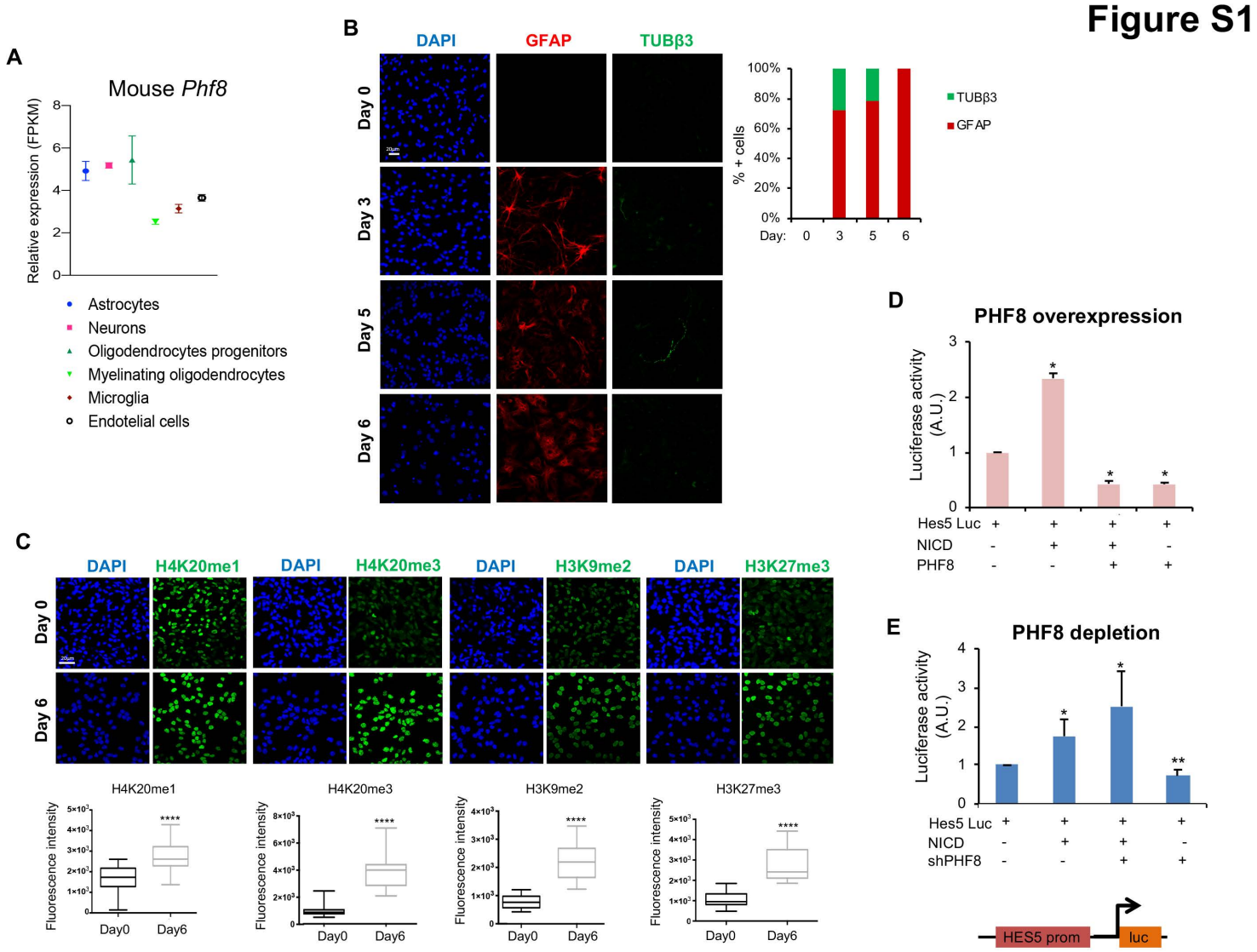

Figure S1. PHF8 expression during astrocyte differentiation

(A) PHF8's expression in different mouse neural cells. Expression level is shown by fragments per kilobase of transcript per million reads mapped (FPKM). Data from public mouse RNA-seq experiments. Available at http://www.brainrnaseq.org.

(B) Immunostaining assay of NSCs maintained in astrocytic differentiation medium for the indicated times using GFAP and TUBβ3 antibodies and DAPI. Scale bar indicates 20μm. Data shown are representative of three biological independent experiments. More than 30 cells per condition were quantified. The graph represents % cells expressing GFAP (red) and TUBβ3 (green) markers at the indicated times.

(C) Immunostaining assays of NSCs (day 0) and astrocytes (day 6). Cells were fixed and stained with H4K20me1, H4K20me3, H3K9me2, and H3K27me3 antibodies and DAPI. Scale bar indicates 20μm. Fluorescence intensity of each histone mark of more than 30 cells was measured using ImageJ. Boxplots represent the quantification of the fluorescence intensity/cell of the histone marks at day 0 and 6. ****p< 0.0001.

(D, E) HEK 293T cells were transfected with a *Hes5* promoter fused to luciferase reporter vector alone or together with NICD, PHF8 or both, as indicated. *Hes5* promoter activity was quantified by the luciferase activity (D). (E) as (D) but shPHF8 vector was used instead of PHF8 expressing vector. Luciferase activity values were normalized to the *Renilla* levels used as a transfection control. Results are the mean of two biological independent experiments. Errors bars represent SD. *p<0.05; **p<0.01 (Student's *t*-test).

Figure S2

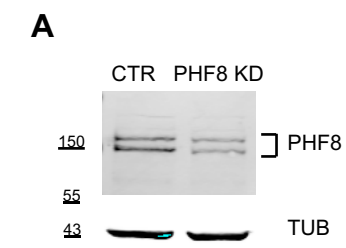

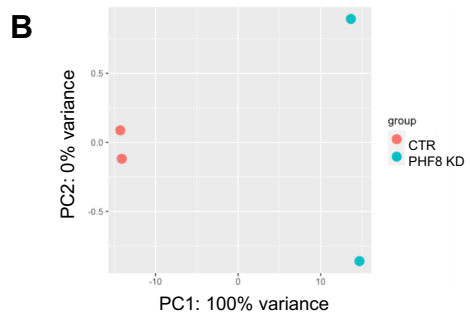

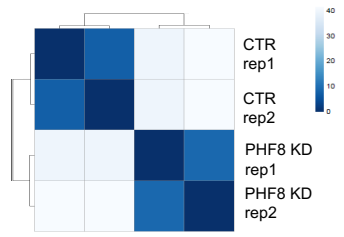

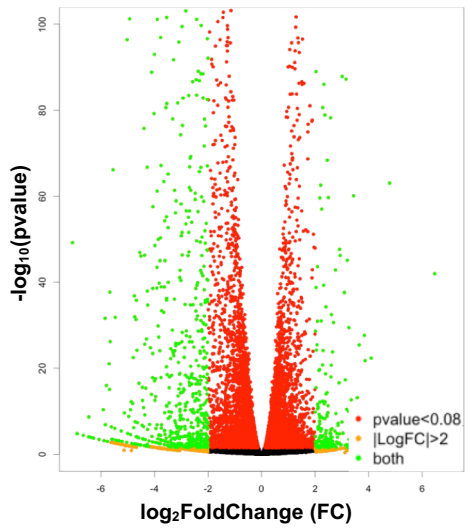

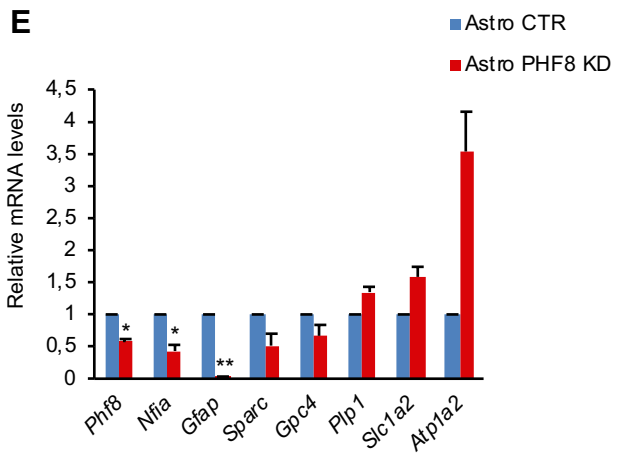

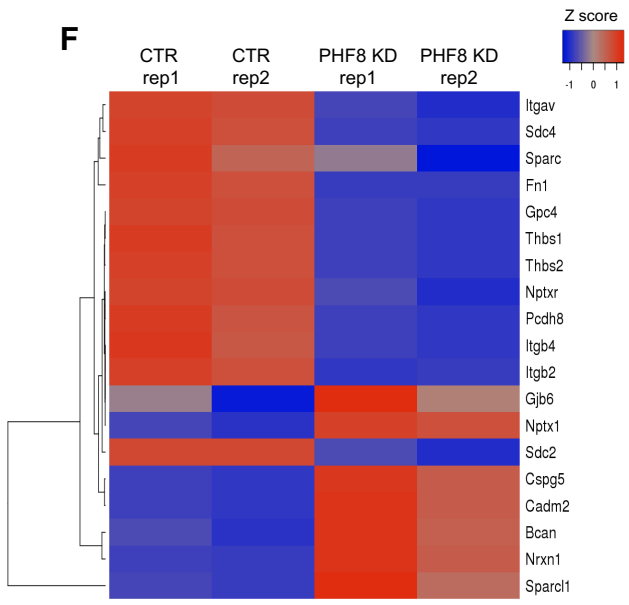

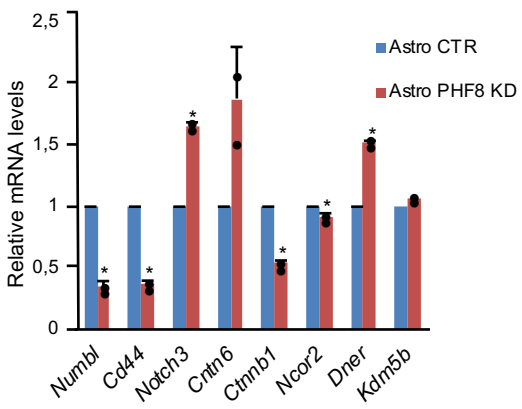

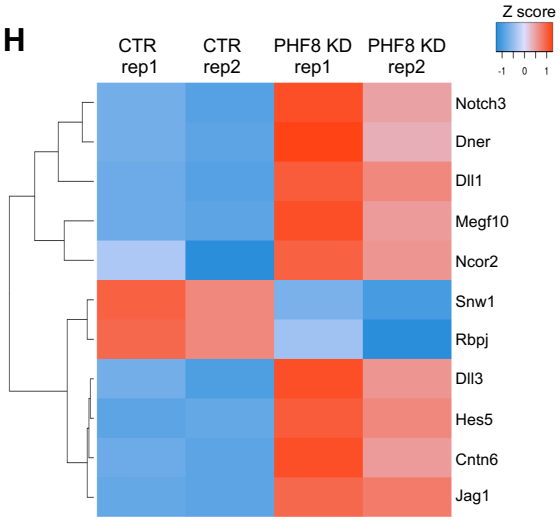

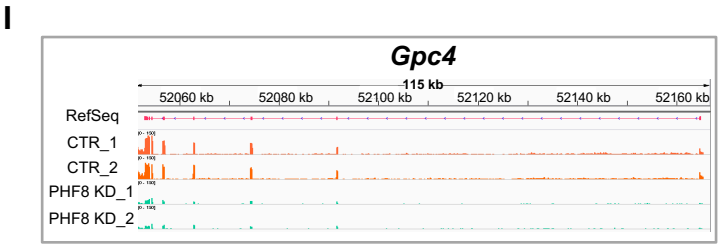

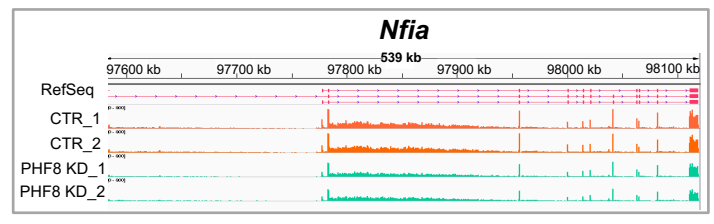

Figure S2. PHF8 regulates transcription in astrocytes

(A) NSCs were infected with lentivirus expressing shRNA control or shRNA specific for PHF8. Total protein extracts were prepared and the PHF8 levels were determined by immunoblot. Alpha tubulin antibody was used as loading control. The immunoblot shown is representative of two biological independent experiments.

(B) Principal component analysis (PCA) plot of normalized RNA-seq read counts. PC1 shows 100% of the total variance and separates treated samples from control samples.

(C) Clustered heat map depicting Pearson correlation of the two samples Astro PHF8 KD and Astro CTR RNA-seq based on read coverage within genomic regions.

(D) Volcano plot displaying the differentially expressed transcripts between CTR and PHF8 KD astrocytes identified by RNA-seq. The green dots represent genes with p-value <0,08 and $\log_2$FoldChange>2 and $\log_2$FoldChange< -2.

(E) Changes of the expression of some selected genes in PHF8 KD vs CTR astrocytes identified in the RNA-seq experiment were validated by qPCR. Values were normalized to the housekeeping gene Gapdh. Errors bars represent SD. *p<0.05; **p<0.01.

(F) Heat map showing some synapse related genes identified by RNA-seq experiment in the two biological replicates of PHF8 KD and CTR astrocytes. All the genes showed p-value<0.08 and log2FoldChange>0.5 and log2FoldChange<-0.5.

(G and J) IGV captures showing RNA levels of *Gpc4* (F) and *Nfia* (I) genes in CTR and PHF8 KD astrocytes.

(H) The misregulation of Notch related genes in PHF8 KD vs CTR astrocytes identified in the RNA-seq experiment was validated by qPCR assays. Values were normalized to the housekeeping gene *Gapdh*. Results are the mean of two biological independent experiments. Values from each of them are indicated by dots. Errors bars represent SD. *p<0.05

(I) Heat map showing some Notch related genes identified by RNA-seq experiment in the two biological replicates of PHF8 KD and CTR astrocytes. All the genes showed p-value<0.08 and log2FoldChange>0.5 and log2FoldChange<-0.5.

Figure S3

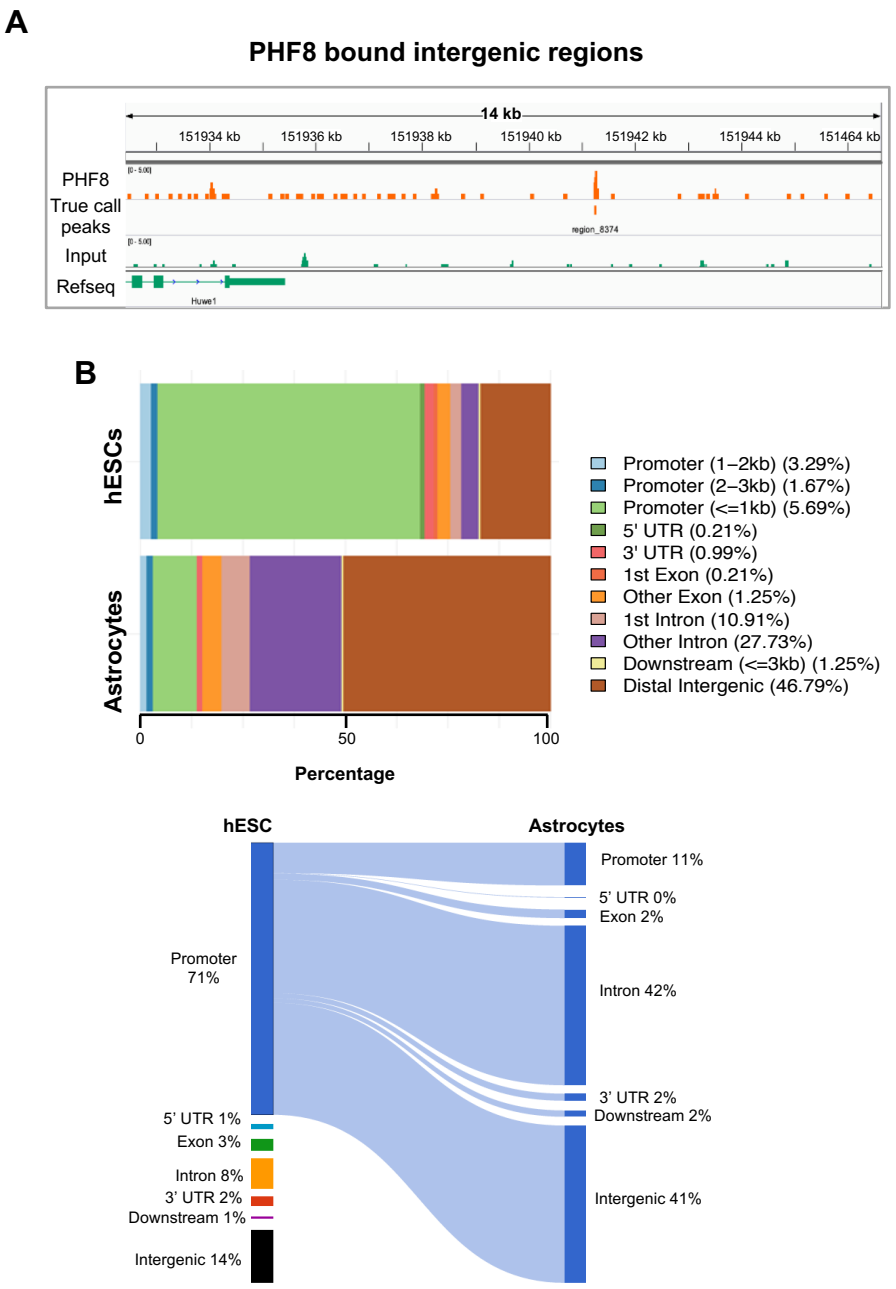

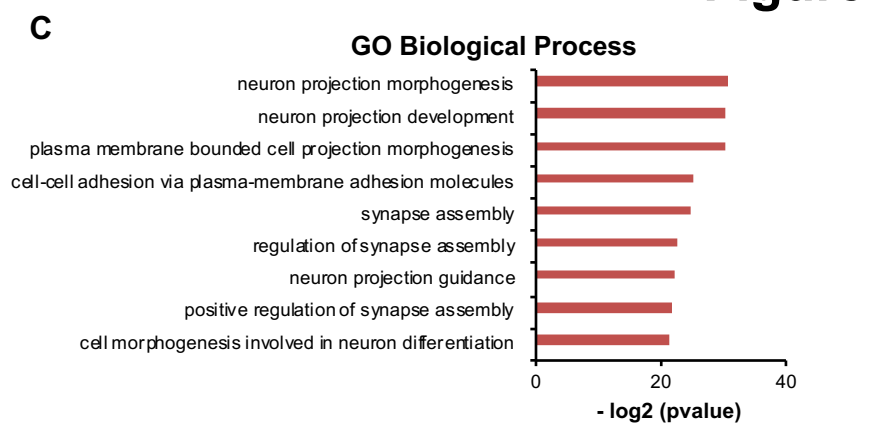

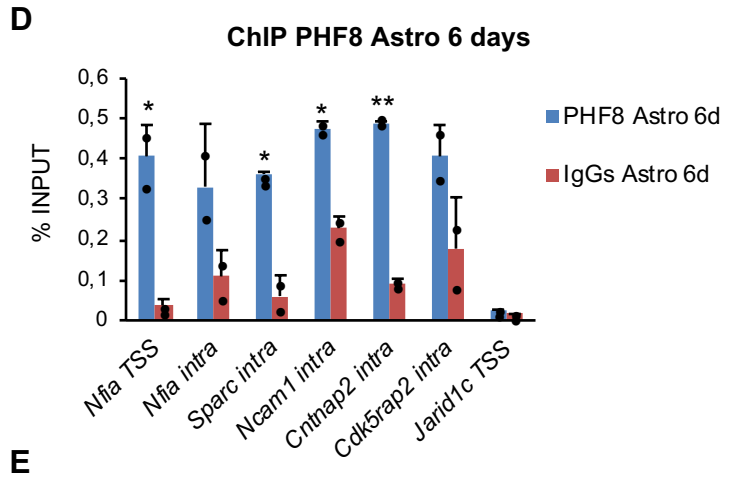

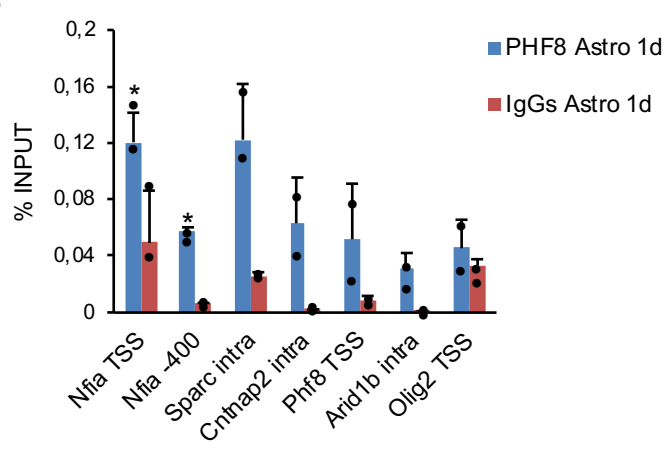

Figure S3. PHF8 binds to astrogenic and synaptogenic genes

(A) IGV capture showing a PHF8 peak in an intergenic region in astrocytes (6 days).

(B) Diagrams depicting the differential genomic distribution of PHF8 in ESCs and astrocytes.

(C) Gene ontology analysis showing Biological Process of the PHF8 bound genes enriched on RBPJ1 motif was performed using as a background the whole Mus musculus genome.

(D and E) The levels of PHF8 at the indicated genes in astrocytes after 6 days (D) or 1 day of differentiation (E) were determined by ChIP-qPCR assays. Data from qPCR were normalized to the input and expressed as % input. *Jarid1c* TSS (C) and *Olig2* TSS (D) devoid of PHF8 were used as negative controls. Results are the mean of two biological independent experiments. Values from each of them are indicated by dots. “Intra” refers to intragenic region identified in the PHF8 ChIP-seq experiment. Errors bars represent SD. *p<0.05; **p<0.01.

Figure S4

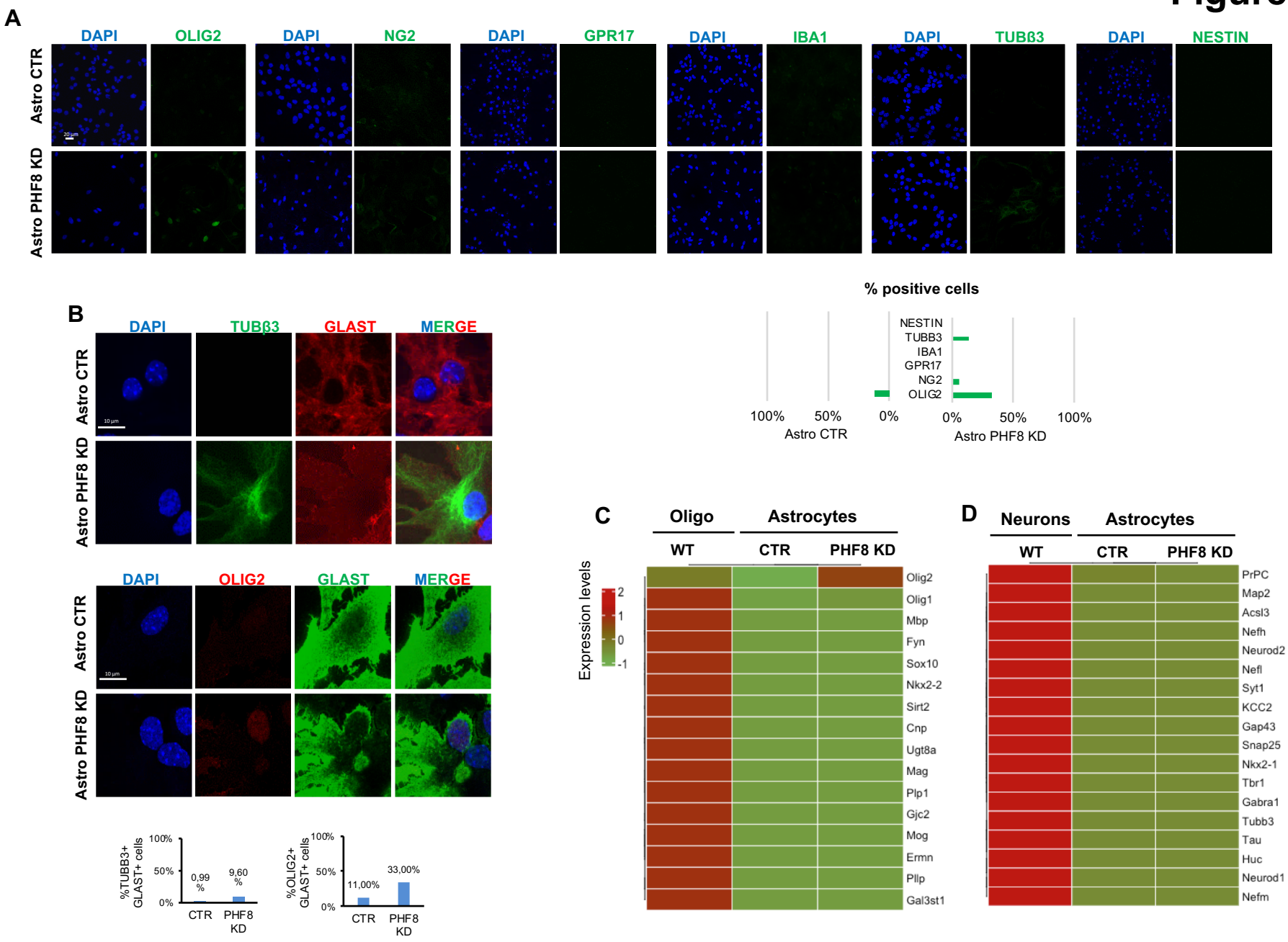

Figure S4. PHF8 depletion alters astrocyte transcriptional profile

(A and B) Control and PHF8-depleted NSCs were differentiated into astrocytes during 6 days to generate Astro CTR and Astro PHF8 KD respectively. Cells were fixed and stained with OLIG2, NG2, GPR17, IBA1, TUBβ3 and NESTIN antibodies and DAPI (A); TUBβ3 and GLAST or OLIG2 and GLAST antibodies were used in (B). The % of cells expressing these markers in each population is shown.

(C-D) Heat maps showing oligodendrocytic (C) and neuronal (D) related gene expression identified by RNA-seq in PHF8 KD and CTR astrocytes compared to oligodendrocytes (GSM1269912, GSM1269911) and neurons (GSM1269905) respectively. Genes showed p-value<0.08 and log2FoldChange>0.5 and log2FoldChange<-0.5.

Figure S5

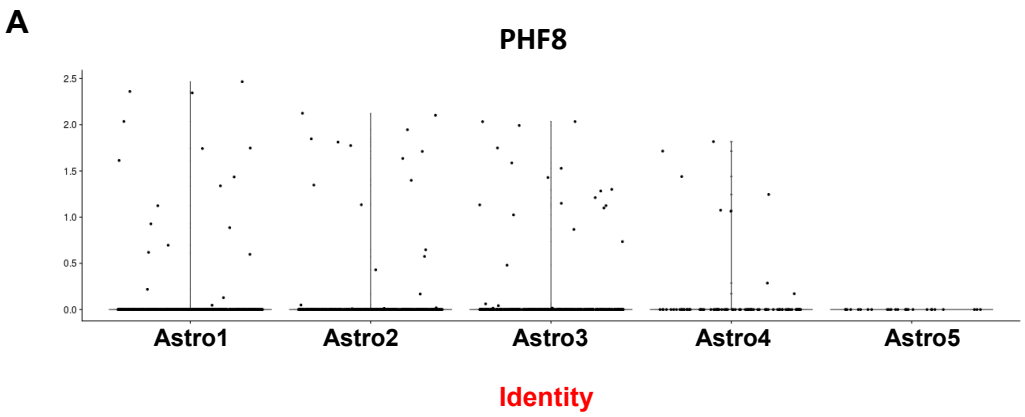

B

Pairwise Intersections

	Atro 2 (126)	Atro 3 (36)	Atro 4 (460)	Atro 5 (217)	Atro PHF8 KD (829)
Atro 1 (37)	0 0.0000	0 0.0000	10 0.0205	3 0.0120	7 0.0081
Atro 2 (126)		4 0.0253	0 0.0000	2 0.0059	22 0.0236
Atro 3 (36)			3 0.0061	2 0.0080	10 0.0117
Atro 4 (460)				50 0.0797	10 0.0078
Atro 5 (217)					9 0.0087

0 Jaccard index 1

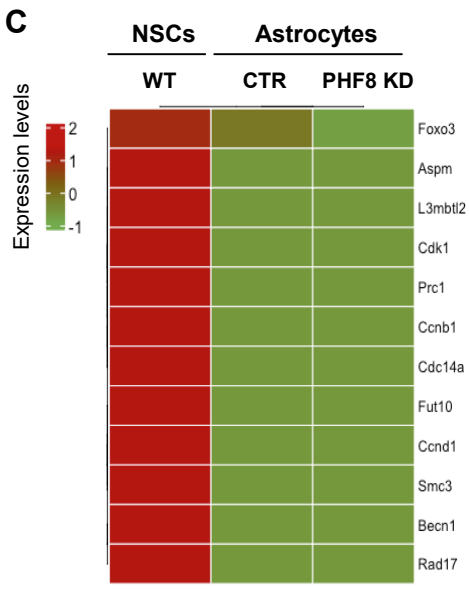

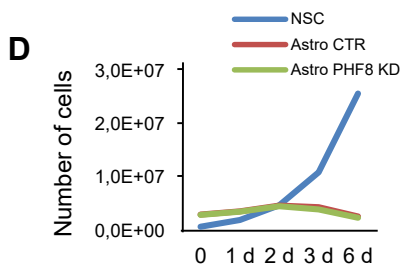

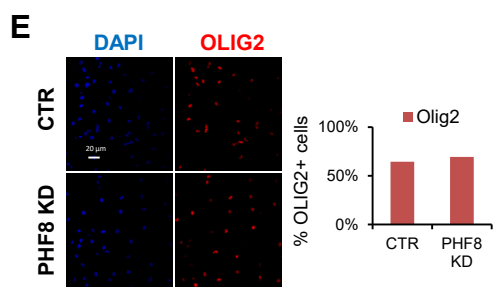

Figure S5. PHF8 depleted astrocytes do not resemble *in vivo* astrocyte subtypes

(A) Data from the public online database https://holt-sc. glialab.org/ showing PHF8 expression in the astrocyte subtypes (Batiuk et al., 2020) in the cortex and hippocampus of adult mice.

(B) Full symmetrical matrix, obtained by molbiotools, showing the comparison between the genes upregulated in PHF8 KD astrocytes and the set of markers that specifically label astrocyte subtypes. Jaccard index indicates the similarity between the samples

(C) Heat maps showing cell cycle and stemness related gene expression identified by RNA-seq in PHF8 KD and CTR astrocytes compared to NSCs (GSE88173). Genes showed p-value<0.08 and log2FoldChange>0.5 and log2FoldChange<-0.5.

(D) Growth curve showing the proliferation rate of NSCs growing in expansion medium and Astro CTR or Astro PHF8 KD growing in astrocyte differentiation medium during 6 days.

(E) Control and PHF8-overexpressing NSCs were maintained in medium without growing factors during 6 days. Cells were fixed and stained with OLIG2 antibody and DAPI. The % of OLIG2-expressing cells is depicted on the right. Scale bar indicates 20μm.

Figure S6

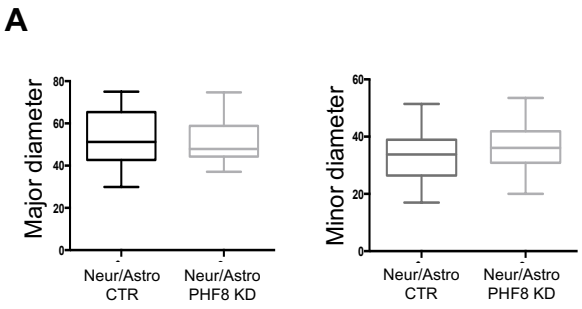

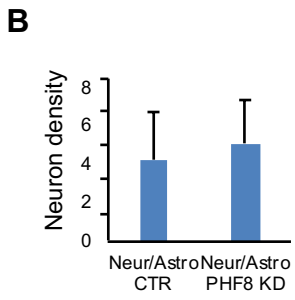

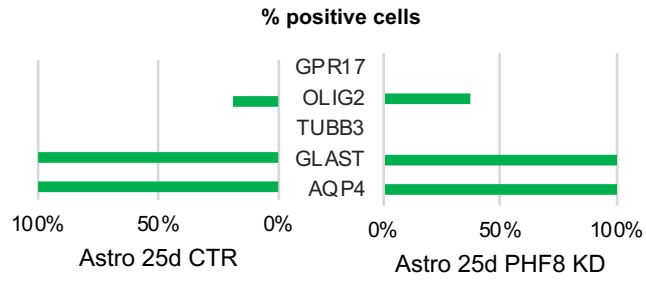

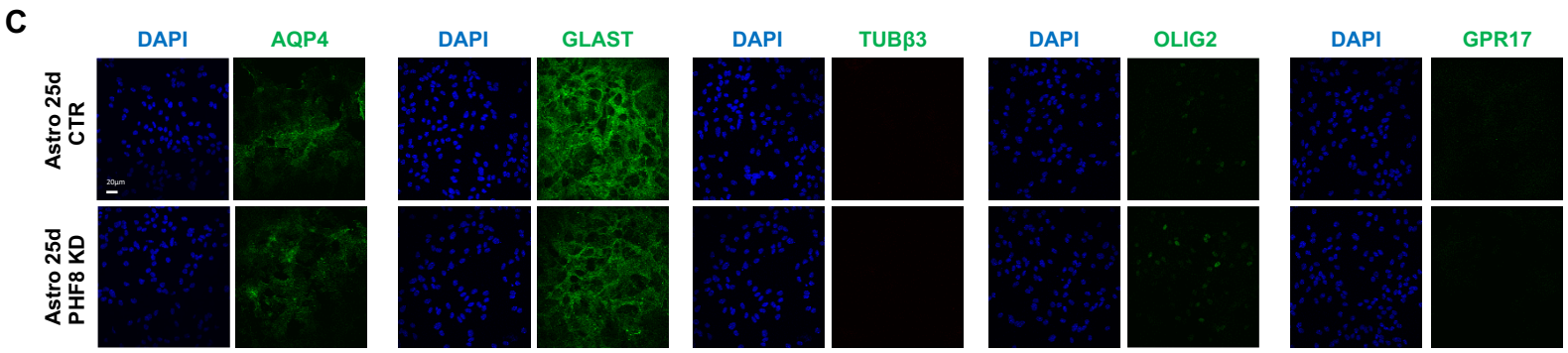

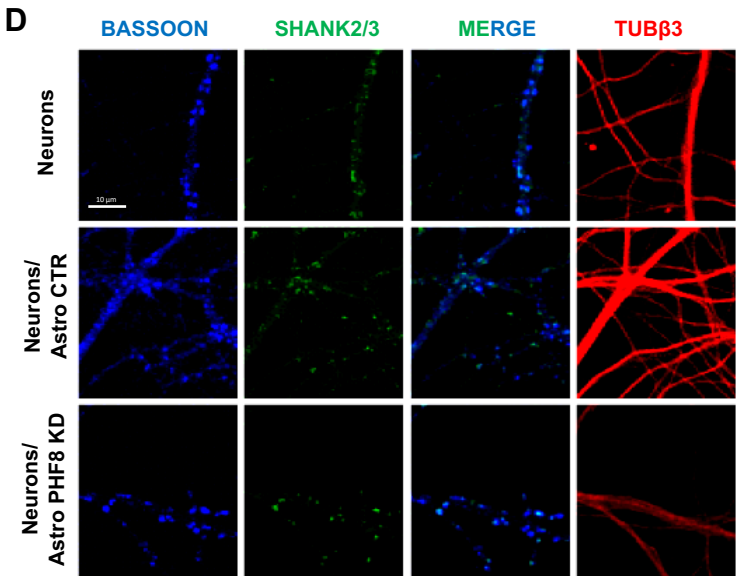

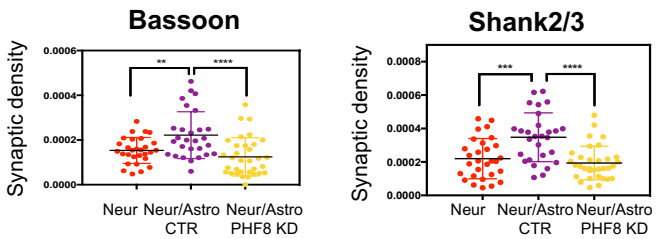

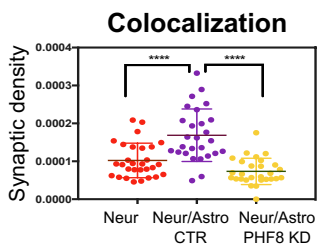

Figure S6. PHF8 depletion impairs neuronal synapse

(A) Analysis of cell body diameter (major, left and minor, right) extrapolated from immunofluorescence confocal for TUBβ3 and DAPI. Major diameter: t-test, p=0.377; minor diameter: t-test, p=0.097; n=31 cells on CTR astrocytes, n=61 cells on PHF8 KD astrocytes.

(B) Neuronal cell density extrapolated from immunofluorescence confocal images of neurons co-cultured with PHF8 KD vs. CTR astrocytes fixed and stained for TUBβ3 tubulin and DAPI. Mann-Whitney Rank Sum Test, p=0.108; n=8 neurons on CTR astrocytes images; n=9 neurons on PHF8 KD astrocytes images.

(C) Immunostaining assay showing the AQP4, GLAST, TUBβ3, OLIG2, GPR17 and DAPI signals in CTR and PHF8 KD astrocytes maintained 25 days in culture. Scale bar indicates 20µm. Quantification showing the % of cells expressing the indicated markers is depicted on the top of the panel.

(D) Immunostaining assay showing the BASSOON and SHANK2/3 levels in neuron cultured without astrocytes, on Astro CTR or Astro PHF8 KD. Scale bar indicates 5µm. The synaptic density was determined by the colocalization of both markers. More than 30 cells per condition were measured. **p<0.01; ***p<0.001; ****p < 0.0001.

Figure S7

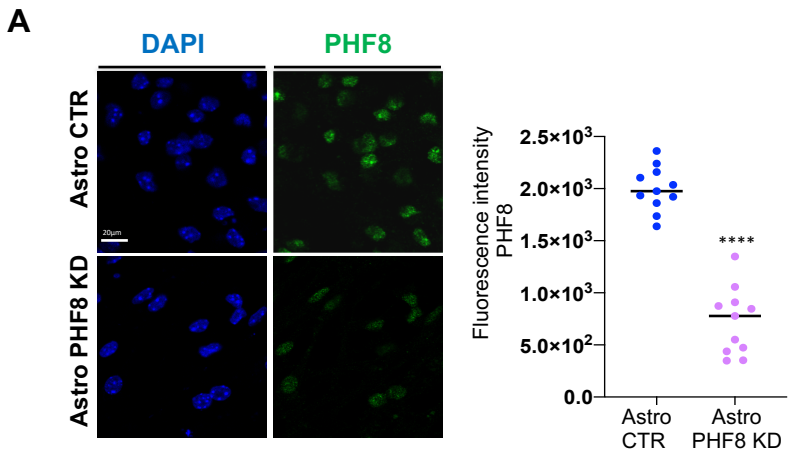

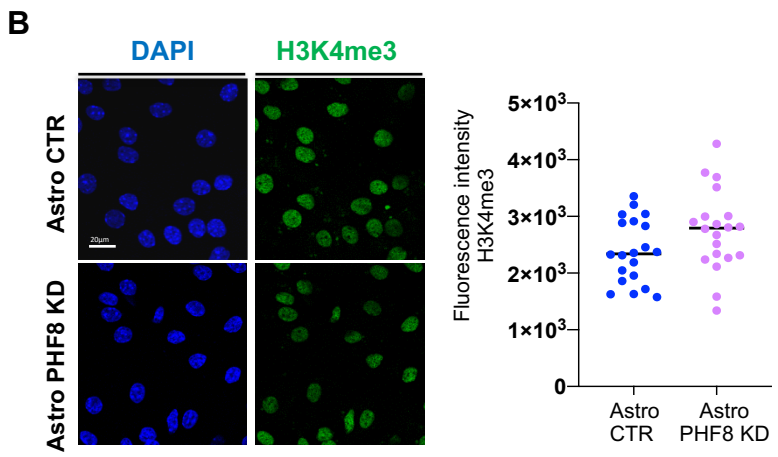

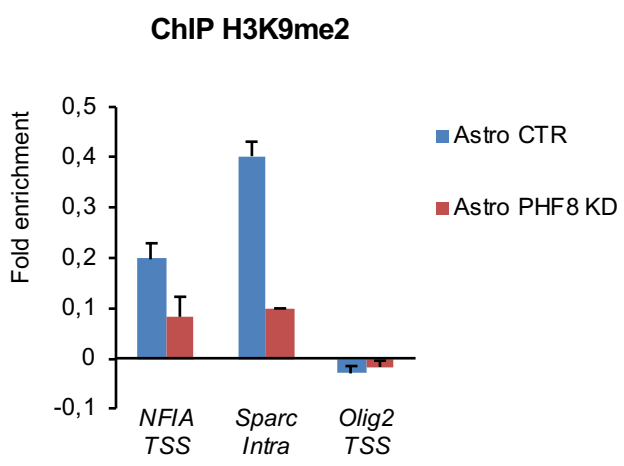

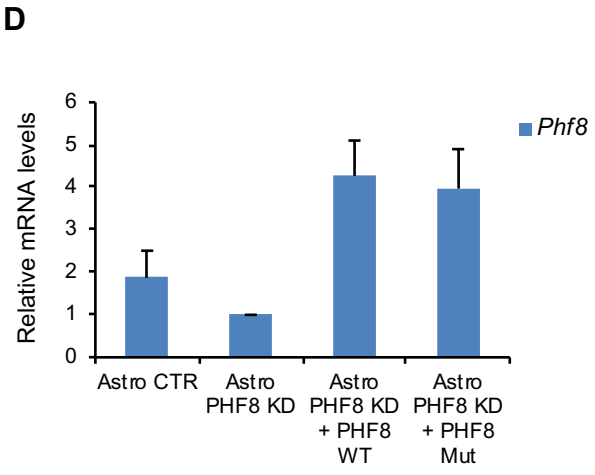

Figure S7. PHF8 maintains low levels of H3K20me1/3 at key astrogenic and synaptogenic genes

(A and B) Immunostaining assay of CTR and PHF8 KD Astro using PHF8 (A) and H3K4me3 (B) antibodies and DAPI. Scale bar indicates 20μm. Images shown are representative of three biological independent experiments. Graphs represent fluorescence intensity per cell.

(C) The levels of H3K9me2 histone mark in CTR and PHF8 KD Astro were determined by ChIP-qPCR at the indicated genes. *Olig2* TSS region was used as negative control. Data from qPCR were normalized to the input and expressed as fold enrichment over the data obtained in shCTR. Results are the mean of two biological independent experiments. "Intra" refers to intragenic region identified in the PHF8 ChIP-seq experiment. Errors bars represent SD. *p<0.05.

(D) PHF8 WT or mutant (H247A) were expressed in PHF8 KD Astro; the level of *Phf8* was determined by qPCR and compared to the level in PHF8 KD astrocytes. Expression values were normalized to the housekeeping gene *Gapdh*. Results are the mean of two biological independent experiments. Errors bars represent SD.

REFERENCES

Batiuk, M.Y., Martirosyan, A., Wahis, J., de Vin, F., Marneffe, C., Kusserow, C., Koeppen, J., Viana, J.F., Oliveira, J.F., Voet, T.*, et al.* (2020). Identification of region-specific astrocyte subtypes at single cell resolution. *Nat Commun* **11**, 1220.

Table S1

Table S1 : List of primers used in this study

Primer sequences	Primer Forward	Primer Reverse
Primers used for gene expression		
Phf8	GCATACTGGAGAACCGAGAG	CGAGATTTCAAAGCAGGGTC
Nfia	CCTCCAACCACATCAACAGAAG	GTACCAGGACTGTGTCTGTTG
Gfap	AGAAAGGTTGAATCGCTGGAG	CTGTGAGGTCTGGCTTGG
S100b	TACTCGGACACTGAAGCCAG	CCCGGAGTACTGGTGGAAG
Olig2	GCTTAGATCATCCCTGGGGC	AGATCATCGGGTTCTGGGGA
Gapdh	ATGTTCGTCATGGGTGTG	CCTTCCACGATACCAAAGTTG
Hes5	CTACCTGAAGCACAGCAAAG	AGCTTCATCTGCGTGTCG
Sparc	TGGATTACTTCGGAGCTTGC	GCTTTTCATTGAGATAGCCGC
Gpc4	ATTGCCCTACACCATCTGC	TCAGCCCATCGTTCATGATC
Dner	AAATGGGATCAAGTAGAGGTGG	AGCAAGATCAGCAAAGAATTGG
Kdm5b	CCTCATATTTACACTCTCCCTTCTC	GTAAGTAGAGTCTGATAAAGCTCCTG
Numbl	CTGAGCCTACGGTTGAATGAG	TTGATGCCATCGCTGTCC
Cd44	CACAACTTCTGGTCCTATGAGG	CTTCTGCCCACACCTTCTC
Notch3	GTAGGCAGAGCAGTGATGTC	GCAGTTGTAAGTATTGACACCG
Cntn6	AGTCTGCCAGTTAATGTCACC	ATCTTGTAGCCCAGCACTTC
Ctnnb1	GTCCTCTGTGAACTTGCTCAG	GTCCTCAGACATTCGGAATAGG
Ncor2	CAAGAAACTCAACACCCACAAC	GGCTTCTACAGGTCATAAGGC
Plp1	CTCCAACCTTCTGTCCATCTG	TGAGTTTAAGGACGGCGAAG
Slc1a2	CAACGGAGGATATCAGTCTGC	TGTTGGGAGTCAATGGTGTC
Atp1a2	GAAAGAGAAGGAGCTCGATGAG	CATCTCTAGCCAGAATGTCCTG
Primers used for ChIP –qPCR		
Nfia TSS	AGCCTGTCATGGGAAATC	ATCAATGGTGTCAGAAAGGT
Nfia -400	TGCAAAGTCTCTTTCAAGCACA	ATCCAATCTAACCCGAGC
Sparcl1 intra	GTGTTAGTGTTCCTTCCGT	AGAGGAAACTCATGAACAGTCAA
Cntnap2 intra	TGCACACACAACATATTCCAC	CACACTCATCCAGATCAATAACTA
Phf8 TSS	TGTTTACCATATCTCTCCACCC	GTTGTAGGAGATTCAAAGCAATCA
Arid1b intra	AGGGAGAGATTCTTAGTCCAT	TTTCATTCAAACGACCGCA
Olig2 TSS	TGCTGCCTCCACCCA	GCTCGGTCTGTAATAAGCAT
Nfia intra	ACCACTGTATGTCTGTGC	CTTCCACTTGGGTTTGTTC
Ncam1 intra	TTCCAGCAAACACTGCAC	AGAAGTCCAATAGTATGCCTGA
Cdk5rap2 intra	CAGTTCGGAGGTCAAAGG	TGATGACTTGAGTTTGATCCC
Jarid1c TSS	TTCCGCCAATGAAATGAACTAT	TCCCTTATTTGGAGGTGGT

Table S2

Table S2 : List of samples used for high throughput sequencing in this study

Sample	Number of replicates	Raw reads count	Average read quality	Aligned reads percent	Aligned reads count	Alignment not unique
RNA shControl _1	Replicate 1	76086389	36,08	96,53	73447385	10,22
RNA shControl_2	Replicate 2	73394533	36,1	96,31	70683464	9,48
RNA shPHF8_1	Replicate 1	82643072	36,11	95,99	79328174	10,36
RNA shPHF8_2	Replicate 2	72624415	36,04	96,14	69820447	8,76
Input PHF8	Control	35980023	36,26	73,4	26410519	33,34
ChIP PHF8	Replicate 1	32546898	36,28	58,22	18950615	24,83